UNIVERSITY OF OKLAHOMA
GRADUATE COLLEGE

DESIGN AND INTEGRATION OF A LOW COST, SIZE, WEIGHT, AND POWER VERTICAL-POINTING SYNTHETIC APERTURE RADAR

A THESIS
SUBMITTED TO THE GRADUATE FACULTY
in partial fulfillment of the requirements for the
Degree of
MASTER OF SCIENCE

By
KURT KONYALIOGLU
Norman, Oklahoma
2022

DESIGN AND INTEGRATION OF A LOW COST, SIZE, WEIGHT, AND POWER VERTICAL-POINTING SYNTHETIC APERTURE RADAR

A THESIS APPROVED FOR THE
SCHOOL OF ELECTRICAL AND COMPUTER ENGINEERING

BY THE COMMITTEE CONSISTING OF

Dr. Jay McDaniel, Chair

Dr. Hjalti Sigmarsson

Dr. Nathan Goodman

Acknowledgments

I would like to thank my advisor, Dr. Jay McDaniel, and my friend, Russell Kenney for their support on this project. I would also like to thank two of my professors - Dr. Hjalti Sigmarsson and Dr. Nathan Goodman - for being crucial learning resources that have helped enable my success on this project.

I also thank my wife Hannah whose support has been key to my success. When the light at the end of the tunnel becomes obfuscated, she is always there to help restore morale.

This work was funded by Sandia National Laboratories, managed and operated by the National Technology and Engineering Solutions of Sandia, LLC., a wholly owned subsidiary of Honeywell International, Inc., for the U.S. Department of Energy's National Nuclear Security Administration under contract DE-NA-0003525.

Table of Contents

List of Tables

List of Figures

Abstract

In modern radar applications, cost, size, weight, and power (C-SWaP) are increasingly becoming critical factors in the design process. For use cases specifically in airborne radio frequency (RF) imaging, there is a key opportunity for improvement in C-SWaP. Typical synthetic aperture radar (SAR) systems consist of aircraft-mounted electronics utilizing an inertial measurement unit (IMU) to provide accurate and precise location information in order to form the synthetic aperture as the aircraft is in flight. Most current SAR applications do not have strict requirements for SWaP since an airframe is capable of handling a sizable amount of weight. With the increased proliferation of smaller airborne vehicles and drones, there is a demand for low C-SWaP radar systems capable of imaging.

In this work, the design and operation of a radar system is discussed. First, basic system requirements including a basic link-budget analysis, and system architecture with low C-SWaP are explored. The analog hardware is then discussed and a RF chain analysis is conducted. The capabilities of the backend module used to capture the data and the IMU used to obtain positional information are then briefly discussed. A basic analysis of the signal processing for SAR is conducted. Finally, results of airborne SAR imaging conducted utilizing the radar system described above are discussed. The system is used in a vertical-SAR (VSAR) configuration as a radar-altimeter to produce an elevation profile of the ground covered by the aircraft.

Chapter 1

Background

1.1 Motivation

Many implementations of Synthetic Aperture Radar (SAR) systems utilize the relatively flexible design constraints afforded by flight platforms such as NASA's DC-8 airliner with a payload capacity of 30,000 lb [1]. With the proliferation of smaller airborne vehicles and commercial drones, there is increased interest in creating imaging radar with lower C-SWaP than previously achievable. As technology advances and high performance commercial-off-the-shelf (COTS) parts become more affordable and available, there is an opportunity to explore improvement in C-SWaP for high performance radar systems capable of imaging.

The design presented is based on a larger connectorized version [2] [3], shown in Figure 1.1, which was used as a proof of concept to vet the system architecture and verify that it is capable of producing a ground-based SAR image which is shown in Figure 1.2. The newly redesigned system is based on X-Microwave's system, a quick prototyping solution for RF components, which allows us to fit the same hardware functionality in a much smaller package while still being reconfigurable. This design is considerably smaller and more portable, allowing for flight tests utilizing a small aircraft operated by the University of Oklahoma's flight

school.

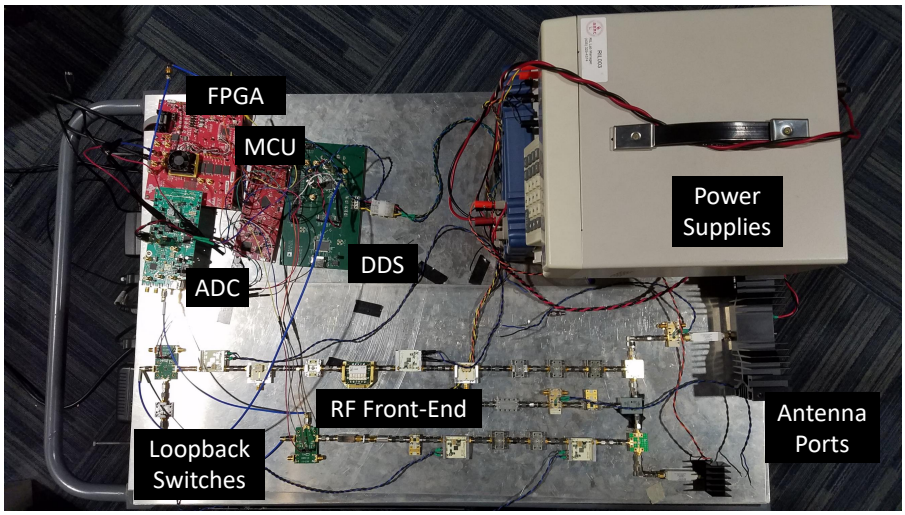

Figure 1.1: Previous connectorized system which this work is redesigning.

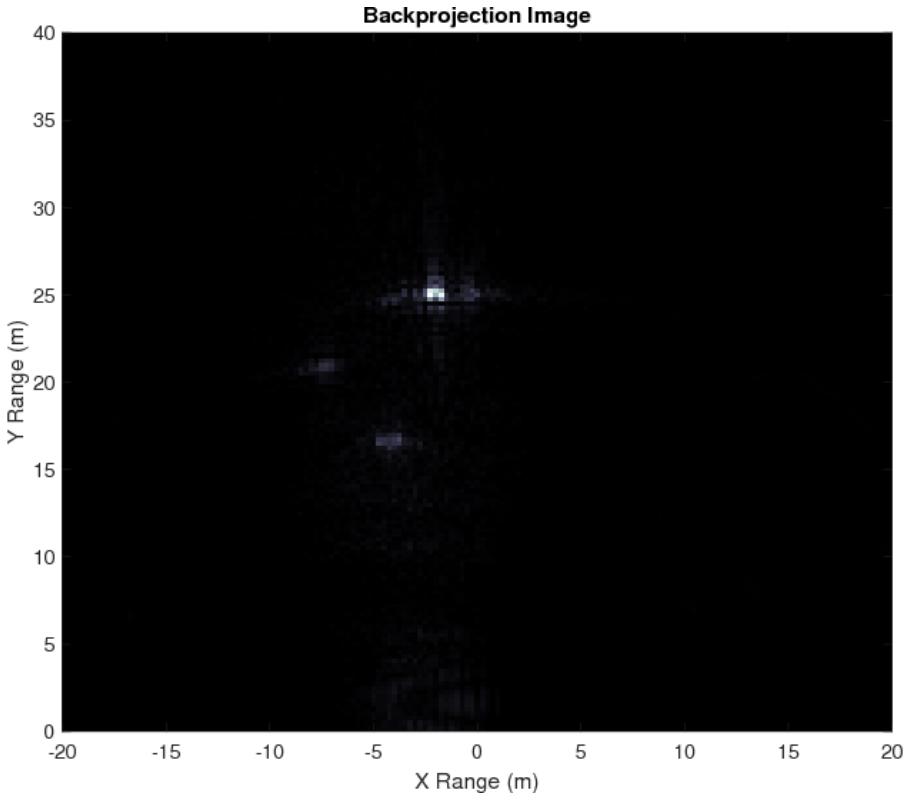

Figure 1.2: Ground-based SAR image of three corner reflectors, produced with previous design.

1.2 Pulse-Doppler Radar

1.2.1 Basic Radar Operation

To provide a baseline understanding for the system in this work, the operation of a typical pulse-doppler radar system will be discussed.

A pulse Doppler radar is able to extract distance and radial velocity information from a target within its scope of operation. The radar transmits a series of pulses spaced out by a period called its pulse repetition interval (PRI), the reciprocal of which is called the pulse repetition frequency (PRF). The length of the pulse is called the pulse width. This concept is illustrated in Figure 1.3.

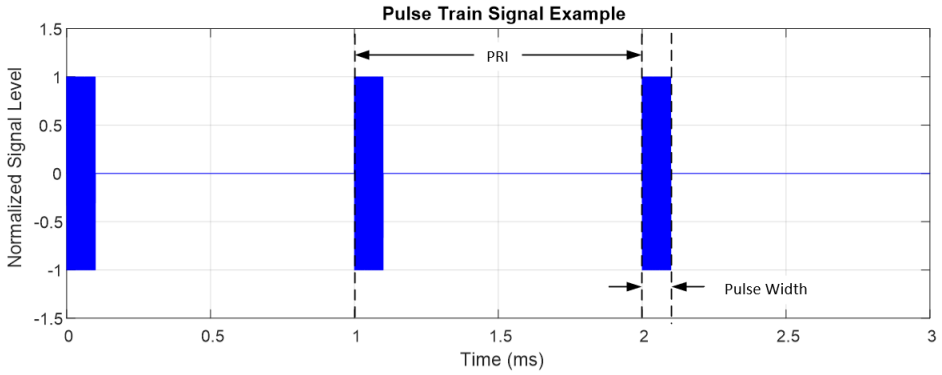

Figure 1.3: Simple pulse train.

The ratio of the pulse width (T_p) to the PRI is the duty cycle. This is important to determine the blind range of the radar (when a radar that is transmitting and is unable to simultaneously receive) and the power dissipation in the system - specifically high power transmit amplifiers that require a low duty cycle in order to operate without special heat mitigation considerations. Distance (R) information is extracted by taking the time between transmitted and received pulse (τ_p also called propagation delay) by where c is the speed of light. This calculates the time it takes

for radio waves to travel $2R$ (to the target and back to the receiver) can be calculated using

$$R = \frac{c\tau_p}{2} \, . \tag{1.1}$$

Note that this implies that the maximum unambiguous range to a target is

$$R_{max} = \frac{c \times PRI}{2} \, . \tag{1.2}$$

The basic equation to calculate range capability of a radar[4] is

$$R_{max}^4 = \frac{P_t G^2 \lambda^2 \sigma}{kT_0 B(NF)(4\pi)^3 (S/N)_{min}} \, , \tag{1.3}$$

where P_t is the transmitted power, G is the antenna gain (assuming transmit and receive paths use an identical antenna), λ is the carrier wavelength, σ is the radar cross section (RCS) of the target (a figure based on how well the target is able to reflect the radar signal), k is the Boltzmann constant, T_0 is the ambient temperature, B is the instantaneous bandwidth, NF is the noise figure, and R_{max} is the maximum detectable range of a given target. Much of the design of a radar system is focused on optimizing these parameters to either increase R_{max} or decrease $(S/N)_{min}$.

Velocity information is extracted by using the Doppler frequency shift (F_D) of the received signal, which is given by

$$F_D = \frac{2v_s}{\lambda_c} \, , \tag{1.4}$$

where v_s is the radial velocity relative to the antenna and λ_c is the wavelength of the carrier[5]. Details of how to extract Doppler information will be given in the section discussing signal processing.

The radar's instantaneous bandwidth (B) also determines the system's range resolution (ΔR) as [5] by

$$\Delta R = \frac{c}{2B} \tag{1.5}$$

and therefore is a critical parameter driving the capability of the system.

1.2.2 Basic Signal Processing

Radar systems typically utilize matched filtering (also called pulse compression) with linear frequency modulation (LFM) in order to pick out the received signal from noise. A matched filter is created by taking the time-reversed complex conjugate of the transmitted signal [5] in the form of

$$h(t) = x^*(T_p - t) \tag{1.6}$$

where $x(T_p - t)$ is the time reversed transmitted signal, delayed by the pulse width, T_p, to ensure the filter does not violate causality. The filter is applied to a received signal, $r(t)$, by

$$y(t) = \int_{-\infty}^{\infty} r(\tau) h^*(t - \tau) d\tau \ . \tag{1.7}$$

When applied to the total received signal, the matched filter shows a peak at a time of the propagation delay plus the pulse width ($\tau_p + T_p$). An example to demonstrate its effect is shown in Figure 1.4. These plots represent a single pulse having been received through a matched filter. The Pulse Width of this baseband signal is T_p = 1 microsecond with a bandwidth of B = 50 MHz.

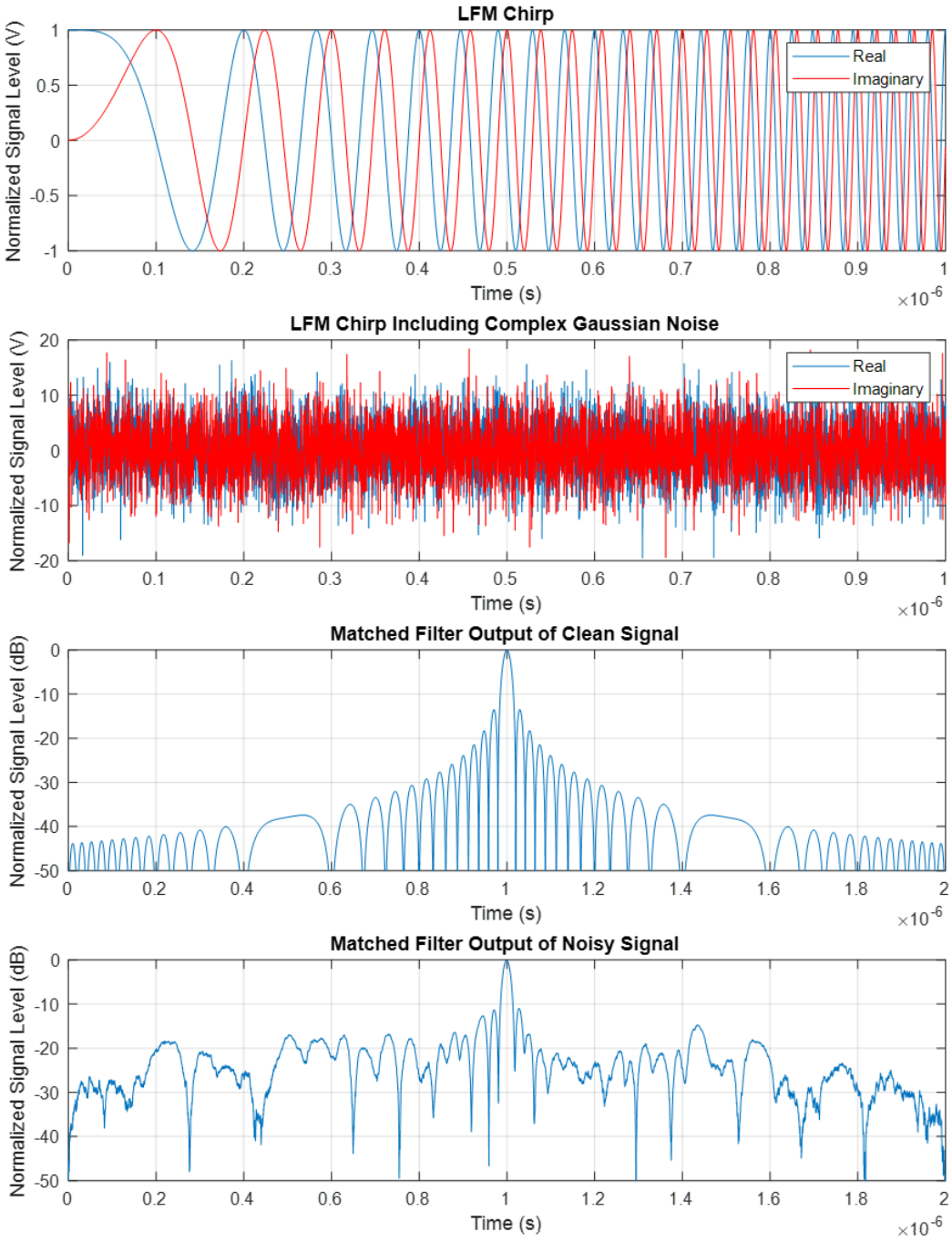

Figure 1.4: Example of LFM chirp and corresponding matched filter output.

Now that we have a single pulse from a matched filter that is able to detect range, we may take samples of multiple pulses at a defined PRF to extract velocity

information. This series of pulses is called a coherent processing interval, or CPI. For realistic targets, Doppler frequency, given by (1.4), is substantially lower than the carrier frequency of the radar. This is exploited to use the PRF of the radar effectively as a sampling frequency for the Doppler shift occurring over pulses. The radar should be designed with a PRF in mind to at least satisfy the Nyquist rate

$$PRF \geq 2 \times F_D \tag{1.8}$$

where F_D in this case is the maximum expected Doppler shift derived from the maximum expected velocity by [5]

$$F_{D,max} = \frac{2 \times v_{max}}{\lambda_c} \, . \tag{1.9}$$

In such a radar, the analog-to-digital-converter (ADC) sample rate is defined as "fast-time", and are discrete samples on the time axis of the matched filter plots shown above. The Doppler sampling defined by the PRF is called "slow-time" since the PRF is typically substantially lower than the sampling rate. This is most easily demonstrated in the range-pulse plot shown in Figure 1.5.

In Figure 1.5, two targets are moving fast enough to travel into different range bins over the course of the CPI. The more range bins a target transitions through, the more "smeared" it will be (in range) on the pulse-Doppler plot. Doppler (velocity) information may be extracted from this plot by measuring the inter-pulse phase change over the CPI by way of a fast-fourier-transform (FFT) over the pulses. Figure 1.5 demonstrates an example of three simulated targets with velocities of 1200 m/s, -800 m/s, and 200 m/s and starting distances of 3610 m, 3590 m, and 3550 m, respectively.

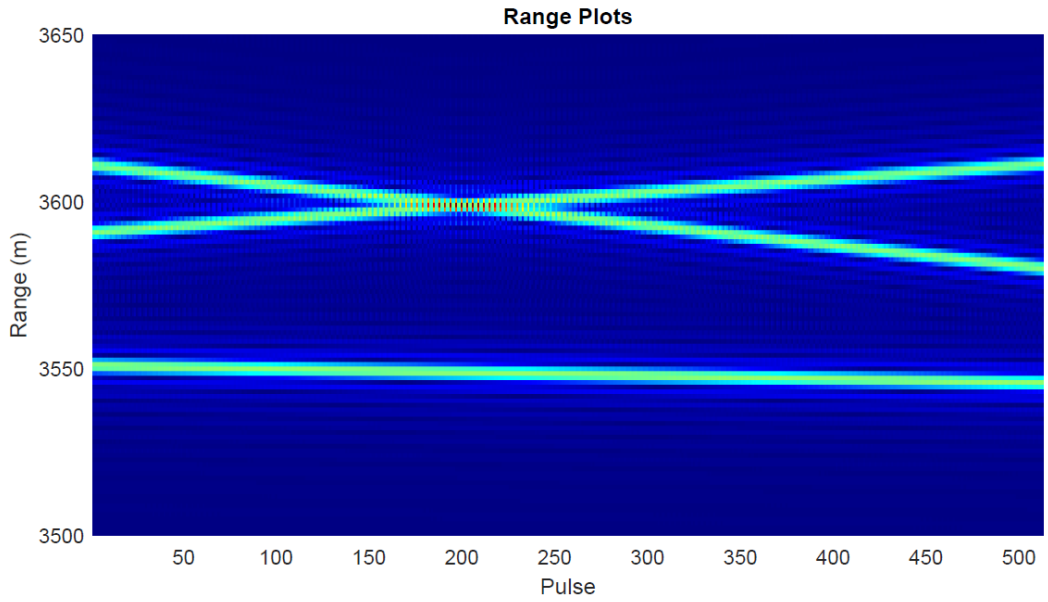

(a)

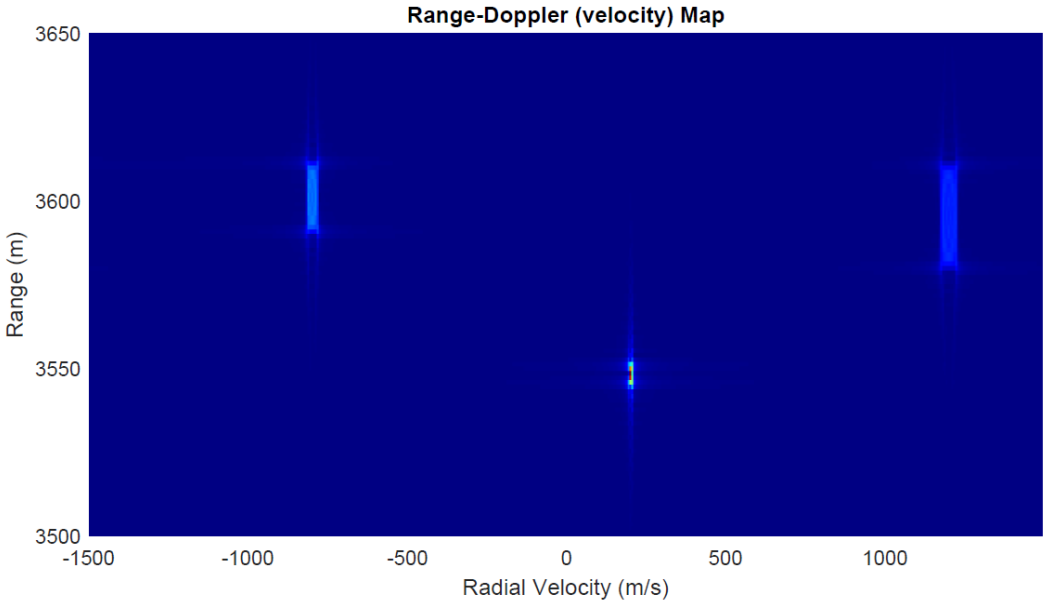

(b)

Figure 1.5: Range-pulse and range-Doppler plots of simulated targets.

1.3 Basic Radar Architecture

This work focuses primarily on the design of the analog-front-end of the radar. In order to transmit, receive, and process a signal in a radar application, one must choose a high level system design that is capable of satisfying design requirements. The simplified architecture for this system is shown in Figure 1.6.

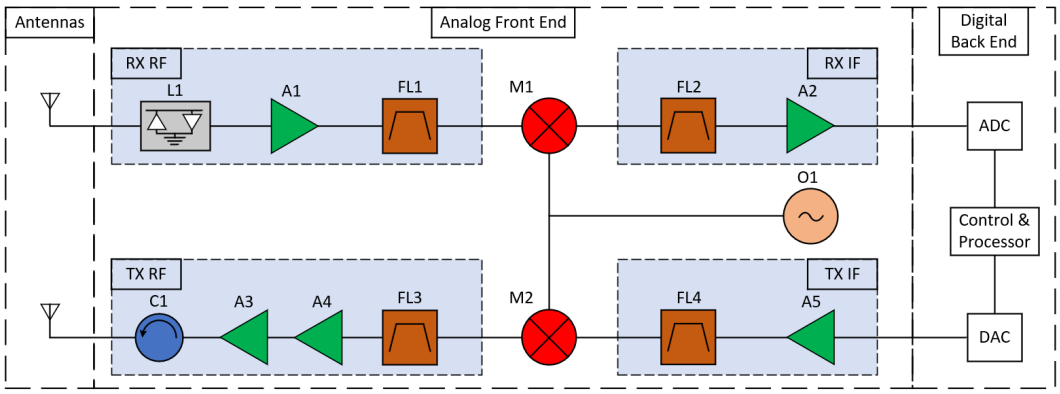

Figure 1.6: Basic radar block diagram.

The key components to factor into the design of the analog front end are shown in Figure 1.6. They are represented as system blocks as opposed to a more detailed hardware block diagram (which will be discussed for this design in a later section). A radar system can be broken up a few ways, but generally the performance-defining system blocks will be the digital back-end, the analog RF front-end, and the antenna or antennas.

The digital back-end generates the baseband waveform (typically a LFM waveform in radar as discussed previously) in the intermediate frequency (IF) range via the digital-to-analog converter (DAC). The signal is then passed through an IF stage (A5 and FL4 in Figure 1.6) to amplify the signal if required and filter any unwanted spectral content that a non-ideal DAC may introduce to the waveform. The signal then passes through a mixer (M2), which modulates the IF waveform onto the

carrier frequency that is generated by the local oscillator (O1) to generate the RF output spectrum. This modulation creates an output that is a multiplication (in time domain) of the local oscillator (LO) and the IF signal. The non-linear process of mixing these frequencies produces many unwanted mixer products that must then be filtered out.

The signal passes through a RF filter stage (FL3) to remove the unwanted mixer products, then moves to a high gain driver amplifier stage (A4) to achieve the optimal input power level for the final stage, the transmit/power amplifier (A3). The system may have a circulator (C1) to protect the output amplifier from a reflected signal if the system is powered on before the antenna stage is connected. Finally, the signal is passed to the antenna which is designed to optimally impedance match the transmission line to free space in order for the signal to propagate in a controlled manner.

On the receive end, the antenna receives the signal, which is then passed through a limiter (L1) that limits the maximum power allowed into the system to avoid damage to the receive components or the ADC. The receive stage must then have a high gain low-noise-amplifier (A1) to ensure noise figure is kept low. Noise factor is given as

$$NF_{system} = NF_1 + \frac{NF_2 - 1}{G_1} + \frac{NF_3 - 1}{G_1 G_2} + ... \tag{1.10}$$

where NF is noise factor, G is gain, and the subscript denotes the order of the component in the signal path. In decibel form, noise factor is called noise figure. As the math implies, the first components in the receiver are the most critical in maximizing signal-to-noise ratio by reducing noise figure, so you want a low-noise high-gain amplifier as early as practical in the receiver's RF stage.

The signal then passes through a filter (FL1) to remove any unwanted spectral

content that is received from sources other than the radar. The signal is downconverted through the receiver's mixer stage (M1), filtered again (FL2), then amplified so the signal is at an acceptable level for the ADC. The signal data is then stored and processed by the back-end solution after being digitized by the ADC.

1.4 System Foundations

In this section, the primary analog components that will drive radar performance will be discussed. It is important to understand what each of these components do and key figures of merit associated with them.

1.4.1 Amplifiers

The primary purpose of amplifiers are to provide gain to raise a signal to a desired level. This is important in order to tune the power at the input of components, such as the ADC, to optimize their performance. Amplifiers, however, are not perfectly linear devices in reality and the nonlinear characteristics must be evaluated during the design process. The most common figures of merit to evaluate non-linear performance characteristics in RF amplifiers are its third-order intercept point (IP3) and its 1 dB compression point (P1dB).

IP3 is the intercept point where a third order product, $2f_{RF1} - f_{RF2}$ for example, reaches the same power level as the desired signal through the component. IP3 is useful to give the designer a rough idea of what IM products to expect for a given component. IP3 may be referenced by input (IIP3) or output (OIP3). The datasheet for a component will typically explicitly state which is being referenced. An example of IP3 is shown in Figure 1.7. A spectrum of two closely spaced tones (RF_1 and RF_2) injected into a system, along with their third order intermodulaton

(IM_3) products ($2RF_1 - RF_2$ and $2RF_2 - RF_1$).

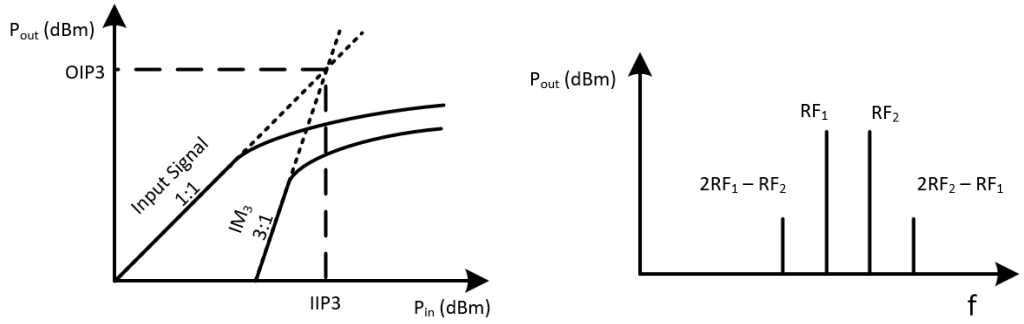

(a) Fundamental and IP3 shown together. (b) IP3 spectrum

Figure 1.7

P1dB is useful to determine how far into the nonlinear gain region (compression) an amplifier is for a given input power. The further an amplifier is into compression, the lower the gain is and the greater harmonic spectral content will be produced as a result of the signal waveform distorting or clipping. Note that there is a output referenced P1dB (OP1dB) and an input referenced P1dB (IP1dB). Typically when the parameter is listed as simply "P1dB", it is referring to the IP1dB since it is a more practical metric for the engineer to use. An example of P1dB is shown in Figure 1.8.

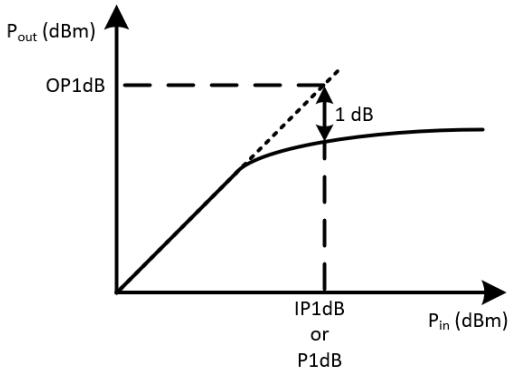

Figure 1.8: Demonstration of P1dB.

There are different types of amplifiers, each with their own optimal application.

Following will be a summary of a few amplifier types in the radar system described in this work:

Low-noise-amplifiers (LNA) are designed to have high gain and high linearity (lower levels of higher order mixing products, which are inherent in active components), and are used most notably in receivers as the primary driver of noise figure. Relevant figures of merit for typical LNAs are: gain, which is maximized to drive system noise figure; noise figure itself to maximize signal-to-noise ratio; IP3; and the P1dB point, which is the point at which the actual output power level differs from the expected output power level assuming linear gain by 1 dB.

Power amplifiers (PA) are designed to maximize the output power and efficiency for the transistor technology. PAs are typically operated at or near compression (beyond the P1dB point) or saturation (well into compression where output power of the device is at maximum) in order to increase power efficiency and maximize power output, using a low-pass-filter to remove harmonics introduced by the IMD products that result from operating in this region if required. Relevant figures of merit for PAs are: output power to meet system requirements; gain to determine required input power for a desired output power; P1dB as a measure of how far into compression the amplifier will be operating; efficiency, since a lot of power may be dissipated in the device; IP3 to determine how much filtering may be required if operating in compression; and overall power draw to determine what mitigation must be in place to prevent heat damage to the amplifier.

Driver, or gain block amplifiers are general purpose and are utilized in a design to bring a signal up to a level which is optimal for downstream circuitry. Typically these are simpler designs where the primary figures of merit are: gain to amplify signal to a level suitable for downstream electronics; maximum output power to ensure it can meet the needs of downstream circuitry; P1dB to ensure you are oper-

ating in a region of linearity that is expected by the system.

1.4.2 Filters

RF filters are used to remove unwanted frequency content from the signal path. A filter is defined first by its ideal transfer function given by

$$H(f) = \frac{V_o(f)}{V_i(f)} \tag{1.11}$$

where $V_o(f)$ and $V_i(f)$ are the output and input voltages, respectively, as a function of frequency (f). The transfer function describes the frequency selective nature of the filter. There are many configurations of filters, but the 4 basic types are shown in Figure 1.9.

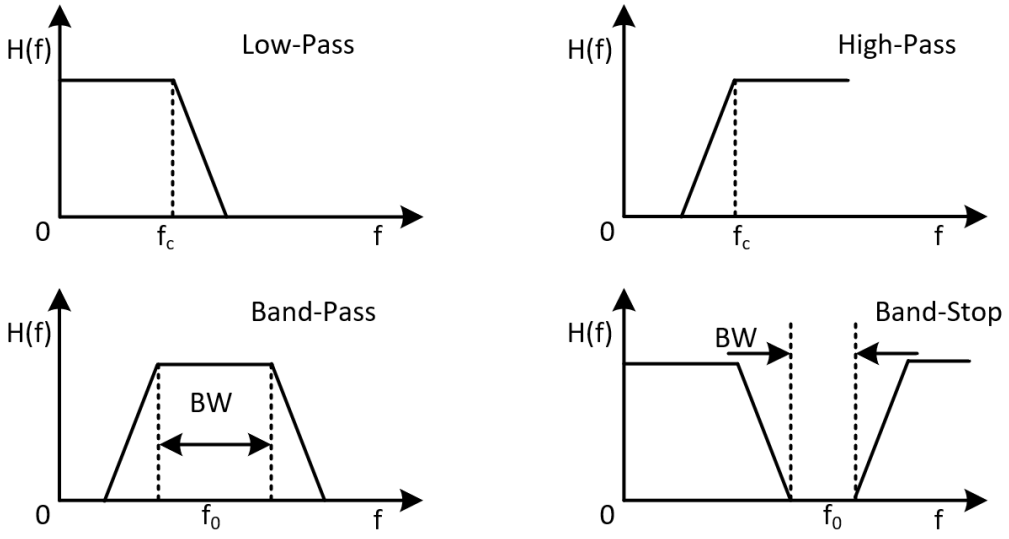

Figure 1.9: Basic filter types.

Briefly describing a few radar use cases for each of these filters: A low-pass filter is typically used to remove harmonics from nonlinearities introduced by active components. A high-pass filter may be used to remove baseband spectral content

that makes it onto the spectrum near the signal band. A bandpass filter is used as an all-purpose filter to select the frequency band the radar signal is operating in and reject spectral content outside of this band. A band-stop filter may be used to remove interference or even the local-oscillator following a mixer, since the local-oscillator frequency will be the most substantial undesired spectral content following such a non-linear process.

In radar applications, COTS filters are selected first based on their frequency band of operation. This is given by the cutoff frequency (f_c) for low-pass and high-pass filters. For band-pass and band-stop filters, this is given by center frequency and bandwidth (f_0 and BW). The cutoff levels vary based on filter topology, but typically a Butterworth is defined using the half-power level, while a Chebyshev is defined by the passband ripple. The rejection of out of band spectral content is evaluated against the system requirements. If no suitable cost-effective COTS filter is available, the engineer may design the filter.

1.4.3 Mixers

In this radar, mixers are used to upconvert signals on transmit, and downconvert signals on receive. Mixers work as an analog multiplier where two input signals (v_1 and v_2) are multiplied and scaled (by $\frac{1}{K}$) for the device's output [6]

$$v_{out} = \frac{v_1 \times v_2}{K} \, . \tag{1.12}$$

The trigonometric identity for multiplied sinusoids is

$$cos(A + B) = cos(A)cos(B) - sin(A)sin(B) \, . \tag{1.13}$$

Suppose that two signals, $v_{RF} = A(t)cos(\omega_0 t + \phi(t))$ and $v_{LO} = A_{LO}cos(\omega_{LO}t)$ are passed through a mixer and multiplied. Applying the trigonometric identity and simplifying, the result is

$$v_{out} = \frac{A(t)A_{LO}}{2}\left[cos((\omega_{LO} + \omega_0)t + \phi(t)) + cos((\omega_{LO} - \omega_0)t + \phi(t))\right] \ . \quad (1.14)$$

It becomes clear that the resulting frequencies are the addition and subtraction of the two signal frequencies in an ideal mixer. In practical application, however, there are an infinite number of mixing products due to the switching nature of mixers [7] given by

$$f_{IF} = nf_{LO} \pm mf_{RF} \ . \quad (1.15)$$

or

$$f_{RF} = nf_{LO} \pm mf_{IF} \quad (1.16)$$

where m and n are all integers. In practice, the fundamental output tones (where $m = n = 1$) are the strongest. There is also loss when modulating the signal from IF to RF or vise versa, called *conversion loss*. An example of mixer operation is shown in Figure 1.10.

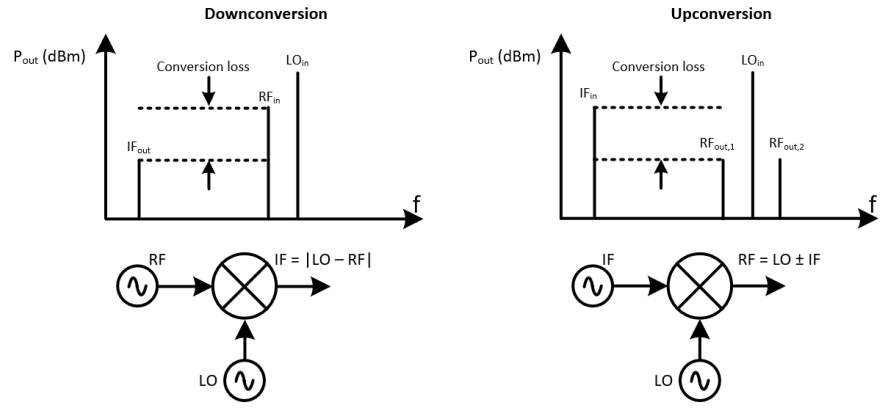

Figure 1.10: Mixer up/downconversion example.

1.4.4 Local Oscillators

The local oscillator used in the front-end of a radar generate the LO signal used in the up/downconversion stages. There are 3 primary parameters to look out for when choosing an oscillator. First is frequency drift. Depending on the timing and application of the radar and whether it interacts with a separate set of hardware, it is important to choose components with a very low frequency drift (depending on the application), or lock the oscillator to a common source to ensure the system remains coherent. System phase coherency is necessary in order to extract phase change information such as Doppler shift over pulses as discussed before.

Another important parameter is the phase noise of the radar. Phase noise, as the name implies, is noise directly affecting the phase of the signal. Poor phase noise performance can result in a reduced SNR. Considering the single tone oscillator signal with frequency f_c, the form can be described as [8]

$$x_c(t) = e^{j(2\pi f_c t + \phi_c(t))} \tag{1.17}$$

where $\phi_c(t)$ denotes the phase noise of the signal. In time domain, phase noise manifests as shown in Figure 1.12. Phase noise changes the signal from a single tone to a distribution in the frequency domain centered at the oscillator frequency. This is shown in Figure 1.11.

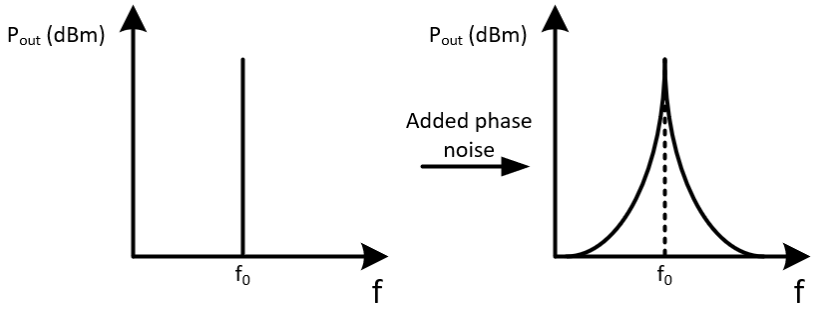

Figure 1.11: Oscillator phase noise example in the frequency domain.

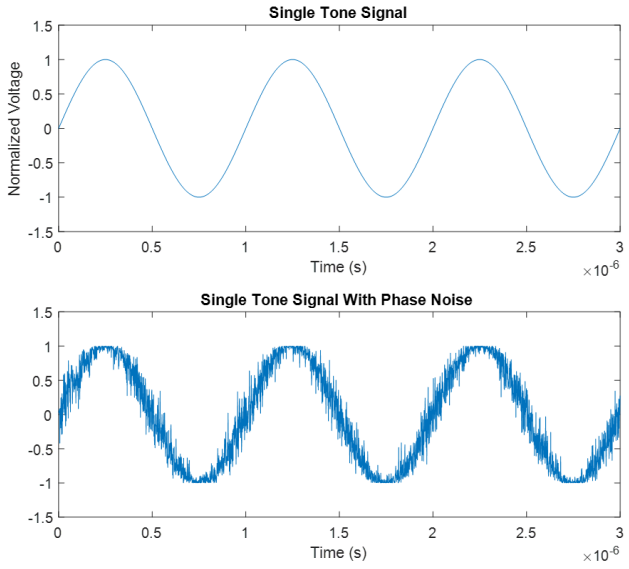

Figure 1.12: Oscillator phase noise example in the time domain.

The last parameter of note with an oscillator is its harmonic level. Since oscillators are inherently nonlinear devices, they contain harmonics (and sometimes subharmonics) of the oscillator's desired output frequency. It is important to factor these harmonics in to the design and filter them out as much as is necessary to meet design requirements.

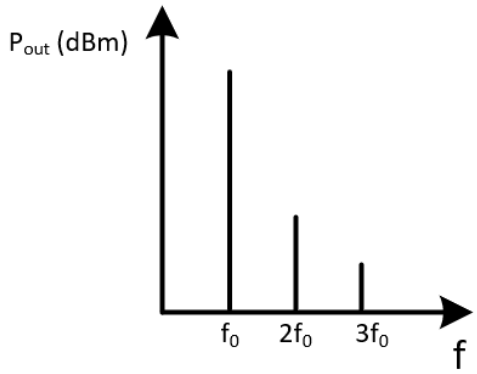

Figure 1.13: Oscillator harmonic example.

1.4.5 Limiters

Limiters prevent power over a certain threshold from passing through the circuit. They are used primarily in receivers in order to prevent damage to components either in the analog receive chain, or the ADC downstream. Limiter functionality is fairly simple in that ideally it will be a through path for the signal. If the signal level is too high, the limiter compresses and saturates the signal, similar to what is shown in Figure 1.8, though typically with a more flat saturated output power level.

A few relevant parameters to consider for limiters are: insertion loss to ensure it doesn't greatly impact noise figure since it will be on the beginning of the receive chain; linear range, or P1dB, to ensure you are working in the linear region of the device; maximum input power; response time to ensure the excessively high signal is limited before downstream components are damaged; and recovery time to ensure the signal is back up in a timely manner after limiting an excessive signal.

1.4.6 Circulators and Isolators

Circulators are 3-port circuits or components that allow an RF signal to pass in one direction, but reflect the signal in the other. Circulators are required in single-

antenna monostatic radar systems so that the transmit signal going into the antenna does not route directly to the receive chain and potentially damage components. Isolators are a 2-port subset of circulators in that one port is terminated to have a "one way street" for the RF signal in the system. Isolators are used in the same manner as circulators, but for multiple antenna or bistatic systems.

Important parameters for circulators and isolators are: insertion loss to reduce noise figure; isolation to ensure a high transmit signal is sufficiently reduced prior to entering the receive chain; voltage-standing-wave-ratio (VSWR) to ensure the transmit amplifier does not see a reflected signal higher than it is capable of handling; forward power to handle the transmit power; and reverse power to handle the transmit power potentially fully reflected back into the device.

1.5 Scattering Parameters

Scattering parameters (or S-parameters) are a mathematical construct that quantifies how energy propagates through a multi-port network. They describe the behavior of voltage and current of an incident wave and a reflected wave at each port of the device. Below is a figure demonstrating a basic 2-port network which will be used to discuss S-parameters.

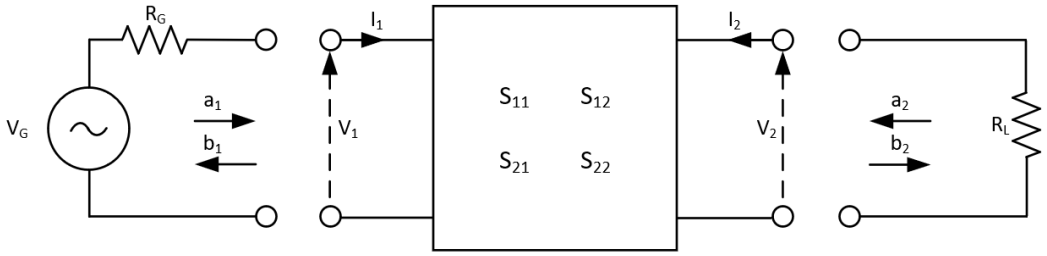

Figure 1.14: A two-port S-parameter network.

Using this model, the basic relationship between incoming waves (a_1 and a_2)

and outgoing waves (b_1 and b_2) is

$$\begin{bmatrix} b_1 \\ b_2 \end{bmatrix} = \begin{bmatrix} S_{11} & S_{12} \\ S_{21} & S_{22} \end{bmatrix} \begin{bmatrix} a_1 \\ a_2 \end{bmatrix} \tag{1.18}$$

To calculate each S-parameter in a practical way which will be used in system simulations, the incoming signal at the unmeasured port is set to zero - note that this implies the system is impedance matched at the unmeasured port with no outgoing signal being reflected from the load. Rearranging to solve for each S-parameter and setting the incoming wave at the unmeasured port to zero results in

$$S_{11} = \frac{b_1}{a_1}\Big|_{a_2=0}, \;\; S_{12} = \frac{b_1}{a_2}\Big|_{a_1=0}, \;\; S_{21} = \frac{b_2}{a_1}\Big|_{a_2=0}, \;\; S_{22} = \frac{b_2}{a_2}\Big|_{a_1=0}. \tag{1.19}$$

To bring this back to voltage values, the following substitutions are made:

$$a_1 = V_1^+, \;\; a_2 = V_2^+, \;\; b_1 = V_1^-, \;\; b_2 = V_2^- \tag{1.20}$$

resulting in

$$S_{11} = \frac{V_1^-}{V_1^+}, \;\; S_{12} = \frac{V_1^-}{V_2^+}, \;\; S_{21} = \frac{V_2^-}{V_1^+}, \;\; S_{22} = \frac{V_2^-}{V_2^+}. \tag{1.21}$$

S-parameters can therefore be used as a ratio of voltages (and by extension, power) to determine the performance of a component in a linear region of operation.

S-parameters will primarily be discussed in the decibel (dB) scale. As such, for the remainder of this work, S_{21}/S_{12} will be referred to as gain (when positive) or insertion loss (when negative). Similarly, S_{11}/S_{22}, which is always less than or equal to zero (between 0 and 1 in scalar), will be referred to as return loss.

Chapter 2

System Design

In this section, a preliminary survey of the operational environment will be conducted and a loose set of system specifications will be derived from it for the analog front-end of the system. The radar itself will be designed to exceed these requirements in order to provide capabilities beyond what the current operational environment requires so that it may be used for future research efforts, however, a baseline set of requirements will be presented as part of the design process.

2.1 Operational Environment

The system will be deployed on small plane flying 1000-2000 ft (300-600 m) in the air to capture data which will be looking between zero and 30 degrees from nadir. This results in a maximum range of approximately 2300 ft, or 700 m. The desired bandwidth for this project is set to 150 MHz as defined by project requirements from the project sponsor. The required output power will be greater than 2 Watts, with a goal of approximately 2.5 Watts. This is what the previous system's transmit amplifier is capable of which will be integrated into this design.

2.2 Link Budget Analysis

A link-budget analysis is necessary to extract the required performance metrics for a prospective radar system. This analysis will be based off of analysis presented in an examination of SAR performance limits [9]. First, start off with the radar equation for a single pulse

$$P_r = \frac{P_t G_A A_e \sigma}{(4\pi)^2 R^4 L_{radar} L_{atmos}} \tag{2.1}$$

where

$$\begin{aligned}
P_r &= Received\ signal\ power\ (W) \\
P_t &= Transmitter\ signal\ power\ (W) \\
G_A &= Transmitter\ antenna\ gain\ factor \\
A_e &= Receiver\ antenna\ effective\ area\ (m^2) \\
\sigma &= Target\ RCS\ (m^2) \\
R &= Radial\ range\ to\ target\ (m) \\
L_{atmos} &= Atmospheric\ loss\ factor \\
L_{radar} &= Microwave\ transmission\ loss\ factor\ due\ to\ system\ losses\ .
\end{aligned}$$

This may also be expressed as

$$P_r = \frac{P_t G_A^2 \lambda^2 \sigma}{(4\pi)^3 R^4 L_{radar} L_{atmos}}\ . \tag{2.2}$$

The noise at the receiver is given by

$$N_r = kTF_N B_N \tag{2.3}$$

where

$$\begin{aligned} N_r &= Received\ noise\ power\ (W) \\ k &= Boltzmann's\ constant = 1.38 \times 10^{-23} J/K \\ T &= Nominal\ scene\ noise\ temperature\ = 290K \\ F_N &= Receiver\ noise\ factor \\ B_N &= Noise\ bandwidth\ at\ the\ antenna\ port\ (Hz)\ . \end{aligned}$$

Calculating the SNR at the receiver antenna port is therefore

$$SNR_{antenna} = \frac{P_r}{N_r} = \frac{P_t G_A A_e \sigma}{(4\pi)^2 R^4 L_{radar} L_{atmos} (kTF_N) B_N}\ . \tag{2.4}$$

When finding the SNR for the image, the gain due to pulse compression and coherent pulse integration must be factored in as

$$SNR_{image} = \frac{P_r}{N_r} = \frac{P_t G_A A_e \sigma G_r G_a}{(4\pi)^2 R^4 L_{radar} L_{atmos} (kTF_N) B_N} \tag{2.5}$$

where

$$G_r = SNR\ gain\ due\ to\ pulse\ compression$$

$$G_a = SNR\ gain\ due\ to\ coherent\ pulse\ integration\ .$$

Considering the monostatic case (which will be configuration of this radar), the transmit antenna gain is given by

$$G_A = \frac{4\pi\eta_{ap}A_A}{\lambda^2} \tag{2.6}$$

where

$$\eta_{ap} = The\ aperture\ efficiency\ of\ the\ antenna$$

$$A_A = The\ physical\ area\ of\ the\ antenna\ aperture$$

$$\lambda = The\ nominal\ wavelength\ of\ the\ radar\ .$$

Integrating this back into the equation gives

$$SNR_{image} = \frac{P_t(\eta_{ap}^2 A_A^2)\sigma G_r G_a}{(4\pi)^2 R^4 \lambda^2 L_{radar} L_{atmos}(kTF_N)B_N}\ . \tag{2.7}$$

Next, factor in gains due to signal processing. Pulse compression gain is due to noise-bandwidth reduction and is given by the time-bandwidth product of the signal

pulse width and the noise bandwidth

$$G_r = \frac{T_{eff} B_N}{L_r} \tag{2.8}$$

where

$$T_{eff} = The\ effective\ pulse\ width\ of\ the\ radar$$
$$L_r = Reduction\ of\ SNR\ due\ to\ non-ideal\ range\ filtering\ .$$

The effective pulse width differs from the transmit pulse width in that it is the portion of the real pulse that makes it into the dataset. This primarily applies to stretch processing, as with a standard matched-filter, the effective pulse width is the actual pulse width. Since stretch processing is not applied in this application, assume that the effective pulse width is equivalent to the transmitted pulse width.

The gain due to pulse integration gain must also be integrated into the equation. The total number of pulses determines the overall gain from pulse integration. This will depend on the PRF in combination with the physical size of the synthetic aperture. The end result of this pulse compression gain is given by

$$G_a = \frac{N}{L_a} = \frac{f_p \lambda R a_{wa}}{2 \rho_a v_x L_a} \tag{2.9}$$

where

$$N = Total\ number\ of\ pulses\ integrated$$

$$f_p = Radar\ PRF\ (Hz)$$

$$\rho_a = Image\ azimuth\ resolution\ (m)$$

$$v_x = platform\ velocity\ (m/s)$$

$$a_{wa} = Azimuth\ impulse\ response\ broadening\ factor$$

$$L_a = Reduction\ in\ SNR\ from\ non-ideal\ azimuth\ filtering\ .$$

Updating the equation yet again yields

$$SNR_{image} = \frac{P_t T_{eff} f_p (\eta_{ap}^2 A_A^2) \sigma a_{wa}}{2(4\pi) v_x R^3 \lambda \rho_a L_{radar} L_{atmos} (kTF_N) L_r L_a}\ . \tag{2.10}$$

Next, the RCS of the distributed nature of the target scene of the SAR will be considered. In this case, it will be expressed as a normalized value per unit area defined by the range and Doppler resolution bins as

$$\sigma = \sigma_0 \rho_a \rho_y = \sigma_0 \rho_a \left(\frac{\rho_r}{cos\psi_g} \right)\ . \tag{2.11}$$

where ρ_y is the ground projected elevation resolution and σ_0 is distributed target reflectivity.

SAR systems are often defined based on a unity SNR for a noise-equivalent scene reflectivity.

$$SNR_{image} = \frac{P_t T_p f_p G_A^2 \lambda^3 \sigma_0 \rho_r}{2(4\pi)^3 R^3 v_x cos(\psi_g) (kTF_N) L_{radar} L_{atmos}} = 1\ . \tag{2.12}$$

Using typical SAR specification values discussed in [9], a distributed target reflectivity requirement of -25 dB (or 0.0032 in linear units) was defined. Since this value based on a Ku-band radar system and since the radar designed in this work operates in this band, this value will be used for simplicity. Without more refined information, assume $L_r = a_{wr} = 1.2$ and $L_a = a_{wa} = 1.2$. The project requirements, which will be used to define downstream system requirements, will be as such: maximum range will be defined as R_{max} = 2300 ft. Flight speed will be approximately v_x = 50 m/s. Grazing angle will be a worst case of $\psi_g > 60°$. Bandwidth as stated previously is set at B_T = 150 MHz, resulting in a $\rho_r = c/(2B_T) =$ 1 m. Pulse width will be set at T_{eff} = 1 μ s with a f_p = 3.012 kHz. Wavelength at 15 GHz will be λ = 0.02 m. Nominal wavelength at the Ku-band frequency of 15 GHz will be approximately λ = 0.02 m. Atmospheric loss, derived from operational environment and range, will be at most $L_{atmos} = 10^{\frac{\alpha R}{10}} = 1.02$, where α is the two-way loss rate from Table 3 in [9] for a clear sky at approximately 5000 ft. For the analysis, L_{radar} is integrated into the noise factor, F_N. Re-arranging the radar equation to use radar system parameters in reference to this noise equivalent reflectivity and integrating the pre-defined system parameters results in

$$F_{N,max} = \frac{P_t T_p f_p G^2 \lambda^3 \sigma_0 \rho_r}{2(4\pi)^3 R^3 v_x cos(\psi_g) k T L_{atmos}} \tag{2.13}$$

which, after plugging in all values, results in a maximum noise factor of approximately 14, or a noise figure of 11.5 dB. The received power was also examined at the maximum and minimum altitude (2300 ft and 1000 ft, respectively) using (2.2) and integrating the other factors discussed above such as pulse compression gain,

pulse integration gain, and grazing angle to get

$$P_r = \frac{P_t T_p f_p G^2 \lambda^3 \sigma_0 c}{4(4\pi)^3 R^3 v_x cos(\psi_g)} \tag{2.14}$$

resulting in a received power (at the antenna output into the receiver) of approximately -84 decibels relative to 1 milli-Watt (dBm) minimum and -72 dBm maximum.

2.3 Backend Considerations

The system parameters above must also be factored into the capabilities of the ADC used in the backend module - the Analog Devices AD9689. The IF frequency will be at 2 GHz. The ADC sample rate is 1.6 GSPS so the IF will be sampling in the third Nyquist zone with at 2 GHz, which is sufficient considering the low bandwidth of 150 MHz. The ideal SNR based on the advertised 14 bits would be 84 dBFS (decibels compared to full-scale) using $SNR = 20\log_{10}(2^{14})$, however non-ideal behavior reduces the actual SNR to 59 dBFS per the datasheet. The maximum input power is calculated using the full scale input voltage $V_{p-p} = 2V$ with $R_{in} = 100\Omega$ as

$$P_{max,dBm} = 10\log_{10}\left(\frac{V_{rms}^2}{R_{in}}\right) + 30 \tag{2.15}$$

to be +7 dBm, where the addition of 30 dB is to convert from dBW (decibels relative to a Watt) to dBm. Using this number with the datasheet SNR results in a minimum input power of -52 dBm.

Now, the approximate range of gain for the system will be calculated. Minimum receiver gain must be 32 dB to get the minimum received power of -84 dBm to the minimum detectable power of the ADC. Maximum receiver gain will be 79 dB to

place the maximum signal level of -72 dBm below the full-scale ADC level at the lowest anticipated altitude of 1000 ft to prevent clipping of the waveform. The spurious free dynamic range (SFDR) of the ADC is 73 dB, so the spur level is set at 70 dBc (decibels relative to carrier) as a baseline requirement to meet the SFDR of the ADC. Also of note is the output power of the DAC of approximately -2 dBm as measured at the device output. For an output power of 2.5W, the required gain is approximately 36 dB total.

2.4 System Requirements

Now, the known system parameters that will affect the front-end hardware and the derived system requirements for the front-end will be consolidated as shown in Table 2.1.

Table 2.1: Front-end system requirements.

Parameter	Value	Units	Description
P_t	2.5	$Watts$	Transmit power
IF	2	GHz	Intermediate frequency
RF	15	GHz	Radio frequency
B_T	150	MHz	Signal bandwidth
$F_{N,max}$	11.5	dB	Noise figure
$G_{rx,max,dB}$	79	dB	Maximum receiver gain
$G_{rx,min,dB}$	32	dB	Minimum receiver gain
$G_{tx,min}$	36	dB	Transmitter gain
$SFDR_{rx}$	70	dB	Receiver spurious free level

Chapter 3

Hardware Design

In this section the design of the analog front-end will be discussed in detail and the digital backend ARENA module from Remote Sensing Solutions will be briefly touched on. The block diagram for the up/downconverter stage will first be examined, then its constituent parts will be discussed in detail. A detailed analysis of the hardware setup using Keysight's Advanced Design System (ADS) will be conducted. In this analysis both linear and nonlinear simulations will be conducted using models available from part manufacturers or ADS models integrating part parameters from datasheets.

3.1 RF Hardware

The RF hardware for this design was selected to minimize the area of the layout while also meeting system requirements with comfortable margin. The components in the new design are utilizing the X-Microwave prototyping solution. This allows rapid testing of RF components and prototyping of RF systems without the cost of fully integrating an RF circuit in a custom board design. The design is loosely based on the benchtop design presented in [3], however the analog hardware has been re-designed to miniaturize and consolidate the system and work within the

new frequency plan. These changes are possible due to the increased capability in the backend ARENA module which will be discussed in a later section. All of the hardware parameters in the following section are based on datasheet values at 25°C.

ZVE-3W-183: Power Amplifier

The Mini-Circuits ZVE-3W-183 amplifier shown in Figure 3.1 was used in the previous design to provide sufficient output power to meet the project requirement of 2 Watts. This part is a Class-A, four-stage, unconditionally stable amplifier which requires a single voltage input of 13-18V and internally regulates voltages for the amplifier gates at each stage.

The connectorized amplifier is again used in the design, primarily to provide sufficient power without requiring additional circuitry designed to sequence start-up power and heat mitigation considerations since the output power is relatively large compared to the rest of the components in the system.

The gain over the bandwidth of interest is approximately 33.5 dB, with a P1dB of 34.5 dBm, an OIP3 of 44 dBm, and a noise figure of 5 dB.

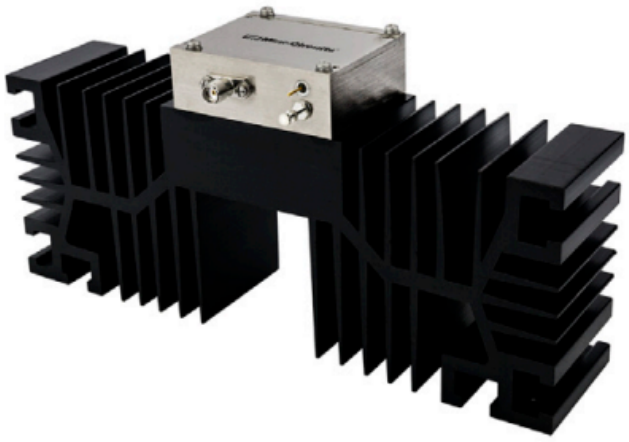

Figure 3.1: ZVE-3W-183 [10].

CMD192C5: Driver Amplifier

The Qorvo CMD192C5 shown in Figure 3.3 is a driver amplifier whose purpose is to bring the transmit signal power up to a proper level prior to passing into the ZVE-3W-183 power amplifier. This part is a wideband GaAs MMIC distributed amplifier in a 5x5mm QFN package with two 0V to -4.0V gate voltage pins whose drain voltage (+8.0 V nominal) is supplied on the RF output pin prior to a DC blocking capacitor. The DC biasing for drain and gate is controlled by an Analog Devices HMC980LP4E bias controller which is on another X-Microwave block mounted on the back side of the RF chassis. The application circuit for the IC is shown in Figure 3.3.

The gain over the bandwidth of interest is approximately 21 dB, with a P1dB of 22.5 dBm, an OIP3 of 30 dBm, and a noise figure of 2.5 dB. A functional block diagram is shown in Figure 3.3.

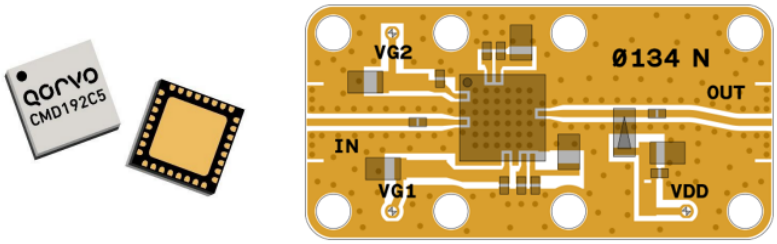

Figure 3.2: CMD192C5 component package [11] and X-Microwave layout [12].

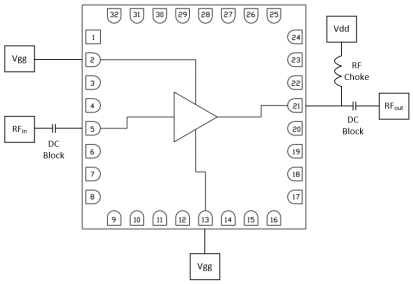

Figure 3.3: CMD192C5 functional block diagram [11] with simplified application circuit.

CMD264P3: Low Noise Amplifier

The Qorvo CMD264P3 shown in Figure 3.4 is a low-noise-amplifier used to bring the received signal to a usable level for downstream components in the receiver. The placement of this amplifier will be the primary determinant of the receiver noise figure. The CMD264P3 is a broadband GaAs MMIC in a 3x3 mm QFN package with a single drain voltage supply pin and internal DC blocking capacitors. This part is powered by a single +3V drain voltage provided by a Texas Instruments LP38798SD voltage regulator on an X-Microwave block on the back side of the chassis.

The gain over the bandwidth of interest is 24 dB, with a P1dB of 12 dBm, an OIP3 of 22.5 dBm, and a noise figure of 2 dB. A functional block diagram is shown in Figure 3.5.

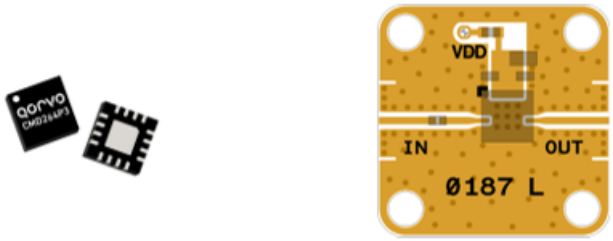

Figure 3.4: CMD264P3 component package [13] and X-Microwave layout [14].

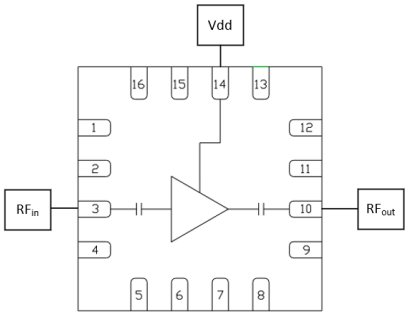

Figure 3.5: CMD264P3 functional block diagram [13].

AVA183A: Gain Block Amplifier

The Mini-Circuits AVA183A shown in Figure 3.6 is a gain block amplifier used to bring the signal power level to a desired window in sections of the RF or LO chains which do not have other specific requirements requiring ultra low noise figure or high power level. It is a wideband, InGaAs PHEMT component in a 3x3mm QFN package with two integrated drain voltage pins. This part requires a +5V supply, which is provided by a Texas Instruments LP38798SD voltage regulator on an X-Microwave block on the back side of the chassis.

The gain over the bandwidth of interest is 13.2 dB, with a P1dB of 19.5 dBm, an OIP3 of 26 dBm, and a noise figure of 5 dB. A functional block diagram is shown in Figure 3.7.

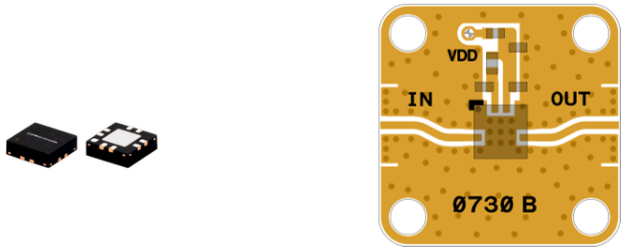

Figure 3.6: AVA183A component package [15] and X-Microwave layout [16].

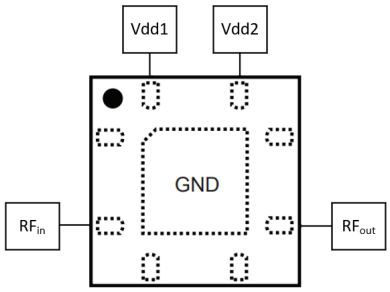

Figure 3.7: AVA183A functional block diagram [15].

TGA2611: Low Noise Amplifier

The Qorvo TGA2611 shown in Figure 3.8 is a low-noise-amplifier which is used as gain blocks in the IF stages of the design. It is a GaN component in a 4x4mm QFN package with integrated drain and gate voltage pins. The required drain voltage is +10V with a nominal gate voltage of -2.3V, both of which are provided by a bias controller using a Analog Devices LT3045EDDTRPBF regulator on an X-Microwave block on the back side of the chassis.

The gain over the bandwidth of interest is 28 dB, with a P1dB of 18.5 dBm, an OIP3 of 29 dBm, and a noise figure of 1 dB. A functional block diagram is shown in Figure 3.9.

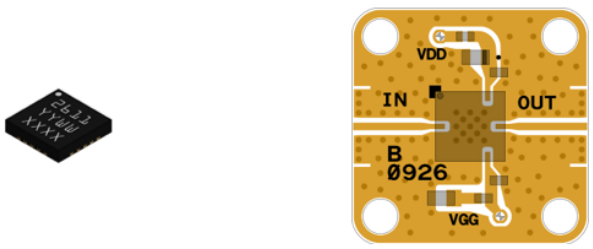

Figure 3.8: TGA2611 component package [17] and X-Microwave layout [18].

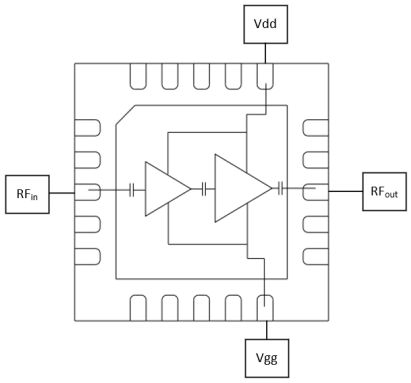

Figure 3.9: TGA2611 functional block diagram [17].

TGL2208: RF Limiter

The Qorvo TGL2208 shown in Figure 3.11 is a dual stage limiter used to protect downstream components from potentially damaging signal levels in the receive chain of the front-end. It is a GaAs VPIN component in a 3x3mm QFN package.

The part has a 1 dB insertion loss, 18 dBm flat RF leakage, and a CW survivability of 5 W. It should be noted that the gain is not flat over signal power level, especially at lower temperatures as shown in Figure 3.11.

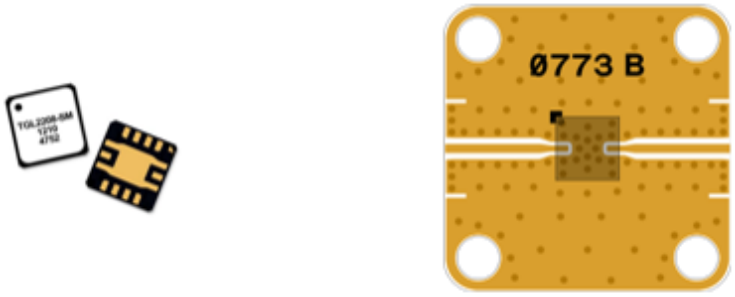

Figure 3.10: TGL2208 component package [19] and X-Microwave layout [20].

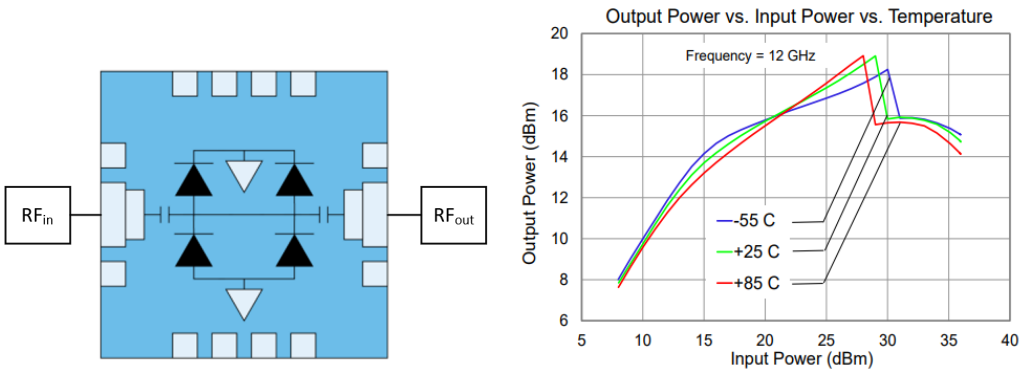

(a) Functional block diagram [19]. (b) Limiting characteristics [19].

Figure 3.11: TGL2208

EP2KA: RF Splitter/Combiner

The Mini-Circuits EP2KA shown in Figure 3.12 is a wideband MMIC RF splitter/combiner used to distribute a coherent local-oscillator frequency to the transmit and receive chains of the front-end. This is a GaAs part on a 3.5x2.5mm QFN package.

The insertion loss is approximately 3.8 dB at the LO frequency, with 15 dB of isolation betweenRF output ports, a maximum of 7 degree phase imbalance, and a maximum of 0.3 dB amplitude imbalance. A functional block diagram is shown in Figure 3.13.

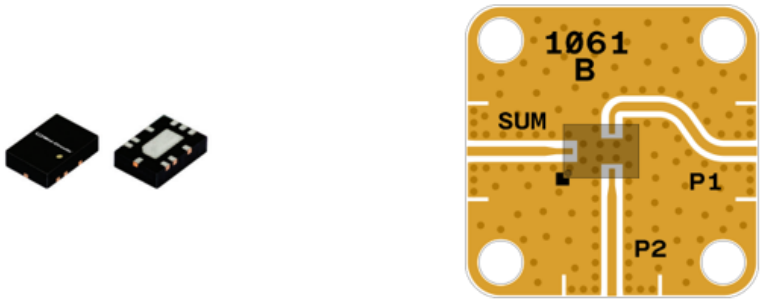

Figure 3.12: EP2KA component package [21] and X-Microwave layout [22].

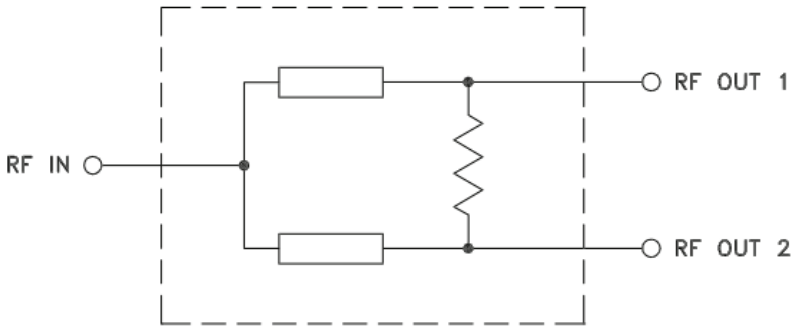

Figure 3.13: EP2KA functional block diagram [21].

CMD178C3: Fundamental Mixer

The Qorvo CMD178C3 shown in Figure 3.14 is a general purpose double-balanced mixer used in the up and downconversion stages in the front-end. It is a GaAs MMIC in a 3x3mm QFN package. With a nominal LO power level of +13 dBm, this mixer has an approximate conversion loss of 6 dB over the band of interest, with 45 dB of LO/RF isolation, 50 dB of LO/IF isolation, and 26 dB of RF/IF isolation. The IIP3 is approximately 16 dBm and IP1dB is 8 dBm - note that these are input referenced as opposed to the output reference for these parameters on amplifiers.

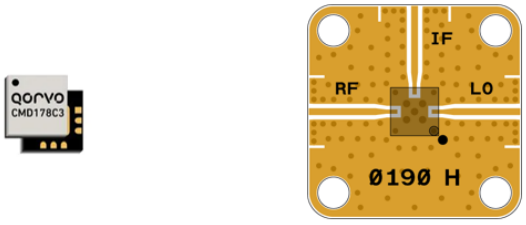

Figure 3.14: CMD178C3 component package [23] and X-Microwave layout [24].

The spurious performance of this component is important in determining the amount of required filtering to sufficiently suppress spurs, so the vendor datasheet must be examined. The spurious levels given in Figure 3.15 will be analyzed both in the preliminary cascade analysis and in the ADS simulation.

	nLO				
mRF	0	1	2	3	4
0	xx	25	33	> 90	> 90
1	28	0	47	40	> 90
2	72	64	64	67	75
3	> 90	> 90	> 90	64	> 90
4	> 90	> 90	> 90	> 90	> 90
RF = 15.1 GHz @ -10 dBm LO = 15.0 GHz @ +13 dBm All values in dBc below the IF output power level (1RF - 1LO)					

Figure 3.15: CMD178C3 spurious outputs at different multiples of LO and RF [23].

ADF5355BCPZ: Wideband Synthesizer

The Analog Devices ADF5355BCPZ shown in Figure 3.16 is a wideband synthesizer with integrated VCO which is used to generate the local-oscillator for up and downconversion in the front-end.

This part has an output frequency range of 54 MHz to 13.6 GHz, so it can sufficiently supply the target LO of 13 GHz. The part is able to directly generate frequencies from 6.8 GHz to 13.6 GHz using the integrated VCO, with the lower frequencies being achieved through a series of frequency dividers.

The specificed harmonic levels for this device are -27 dBc (second) and -20 dBc (third). Phase noise is specified as approximately -103 dBc/Hz, -124 dBc/Hz, -126 dBc/Hz, and -144 dBc/Hz at 100 kHz, 800 kHz, 1 MHz, and 10 MHz offset from carrier, respectively.

The part requires a +3.3V supply for both digital and analog parts, with a nominal VCO power supply of +5V, both of which are provided by an Analog Devices ADF5355BCPZ regulator on an X-Microwave block on the back side of the chassis. A 10 MHz reference clock is provided both to this synthesizer and the backend ARENA module to allow phase coherency and mitigate frequency drift between all system parts. The output power at the local-oscillator frequency is approximately 0 dBm.

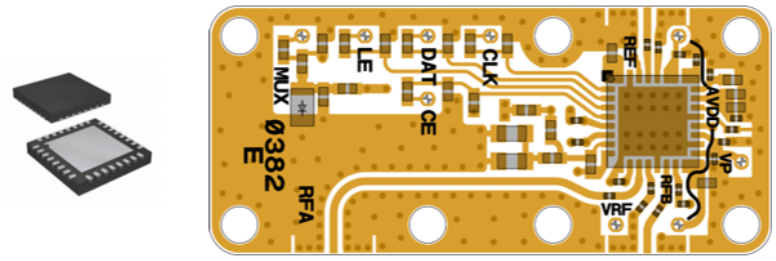

Figure 3.16: ADF5355BCPZ component package [25] and X-Microwave layout [26].

XM-B9B4-1404D: RF Band Pass Filter

The X-Microwave XM-B9B4-1404D shown in Figure 3.17 is a cavity bandpass filter with a 161 MHz bandwidth, selected to cleanly pass the RF frequency band centered at 15 GHz. The insertion loss within the passband is approximately 3 dB, with 20 dB rejection points at 14.85 GHz and 15.12 GHz.

This filter would suppress LO leakage in the RF chain by 75+ dB, which is more than sufficient to satisfy the SFDR when combined with the 45 dB LO/RF isolation of the mixer. The image of the RF frequency (at 11 GHz) would also be suppressed by 75+ dB. The filter has 60 dB of rejection out to 42 GHz with very little flyback, so it would sufficiently remove any second order harmonic content in the RF chain. The S-parameter performance is shown in Figure 3.18

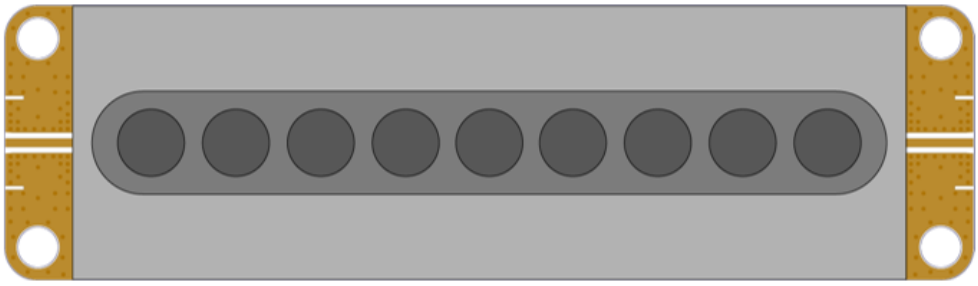

Figure 3.17: XM-B9B4-1404D X-Microwave layout [27].

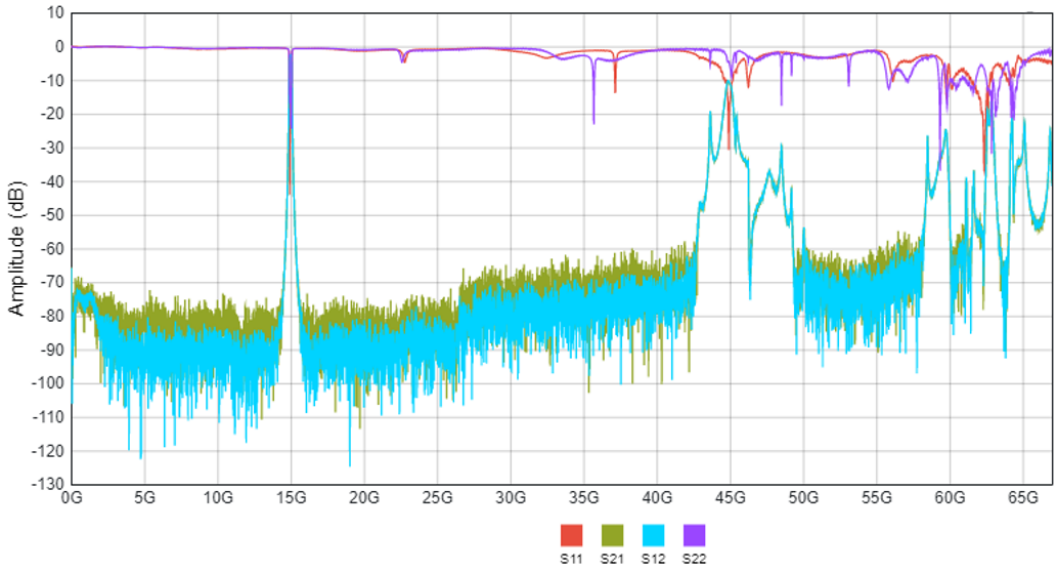

(a) Broadband performance.

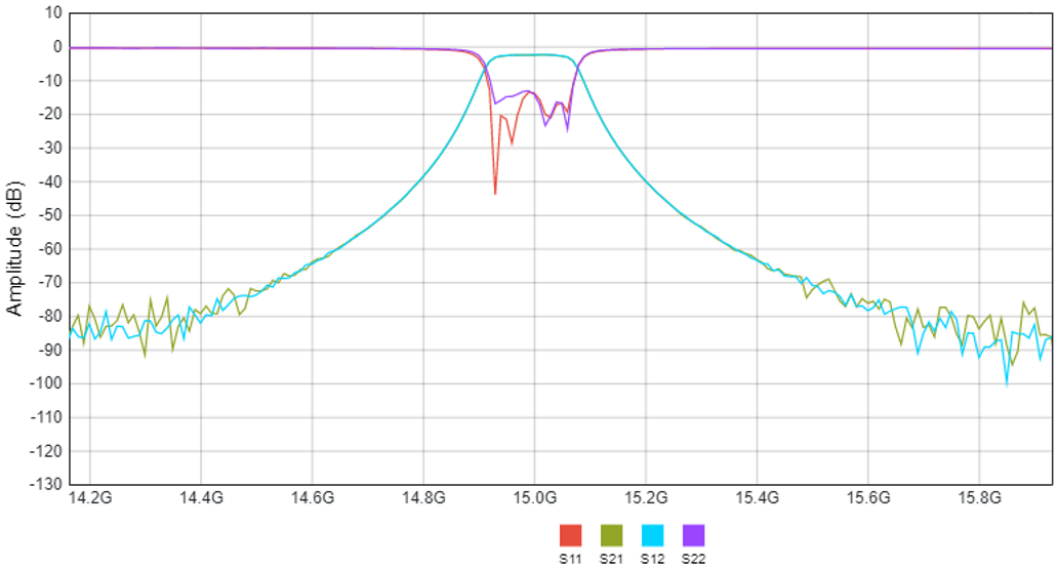

(b) Narrowband performance.

Figure 3.18: XM-B9B4-1404D [27]

L204XF4S: RF Low Pass Filter

The Dielectric Labs L204XF4S shown in Figure 3.19 is a high-Dk ceramic surface mount low pass filter optimized for Ku-band performance. The cutoff frequency of this filter is approximately 20.6 GHz, with a passband insertion loss of 1.1 dB in the band of interest, as shown in Figure 3.20. The filter rejection at the second harmonic (30 GHz) is 50+ dB. This filter was selected to remove harmonics in the transmit chain caused by operating close to the non-linear region of the driver amplifier.

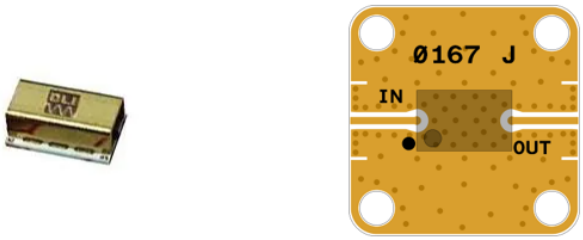

Figure 3.19: L204XF4S Package [28] and X-Microwave layout [29].

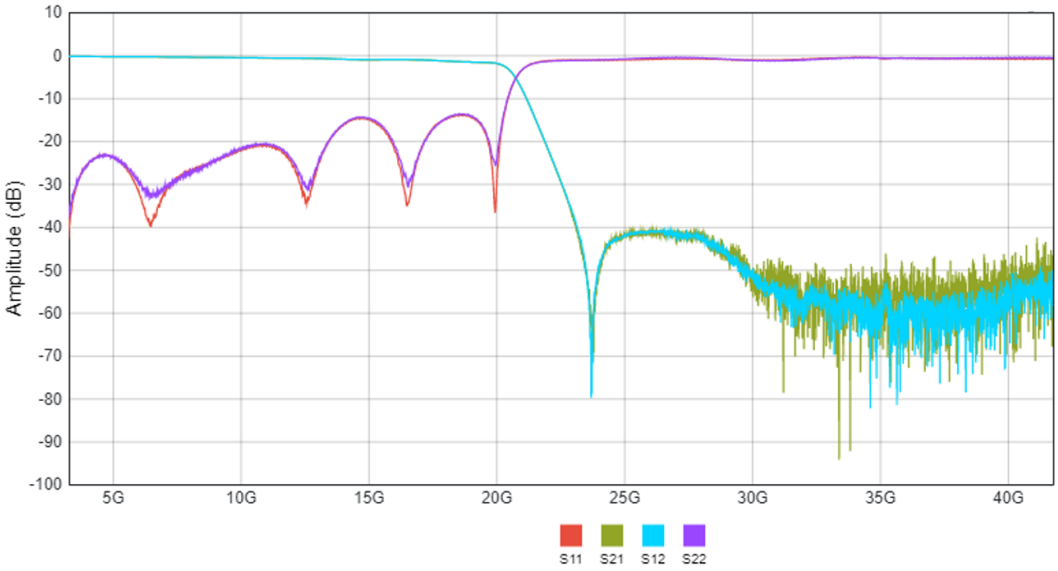

Figure 3.20: L204XF4S S-parameter performance [29].

HFCN-1600: IF High Pass Filter and LFCN-2250: IF Low Pass Filter

These two ceramic SMT Mini-Circuits filters (HFCN-1600 and LFCN-2250, shown in Figure 3.21) were used in combination for a band pass effect in the IF frequency band, creating a passband of 1600 MHz to 2250 MHz. The purpose of these filters on the TX chain is to remove any unwanted spurious content from the ADC, especially any harmonic content. The purpose of these filters on the RX chain is to reject any unwanted mixing products and leakage after downconversion. Typically it is best to avoid using cascaded filters due to the impedance mismatch outside of the passband creating undesirable effects, however these filters were tested together to verify that there are no such issues. The insertion loss for both of these filters is approximately 1 dB. Performance is shown in Figure 3.22.

Figure 3.21: HFCN and LFCN Package [30] and X-Microwave layout [31].

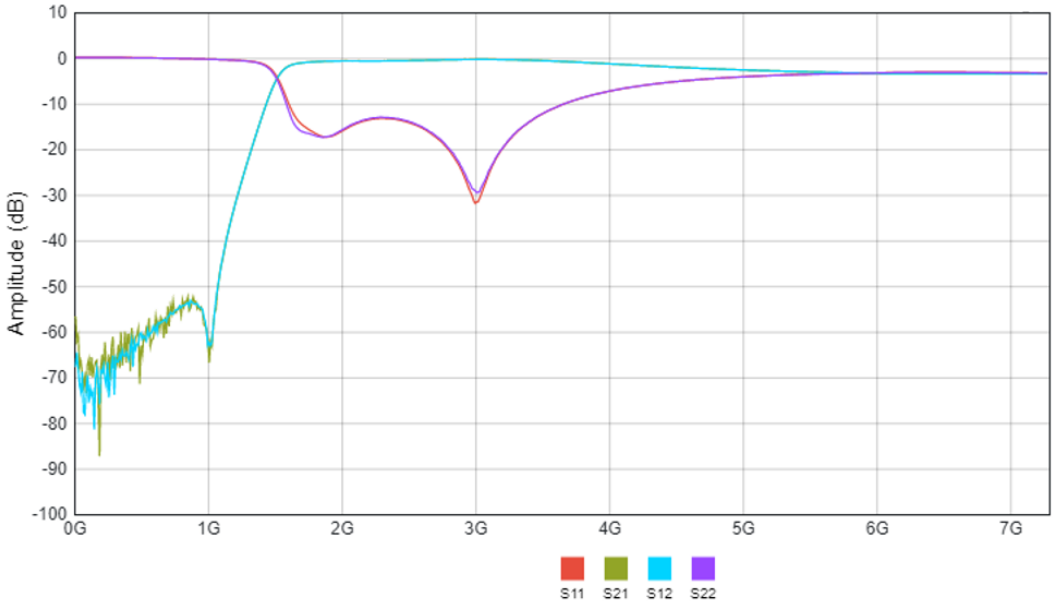

(a) HFCN-1600 S-parameter performance [31].

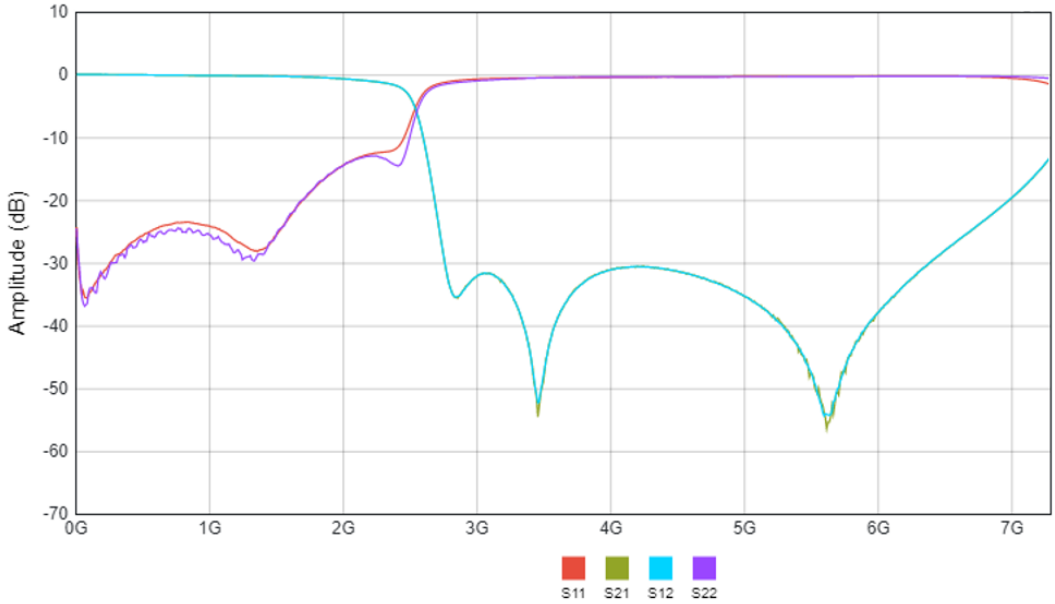

(b) LFCN-2250 S-parameter performance [32].

Figure 3.22: Mini-Circuits Filters

XLF-252: IF Low Pass Filter

The Mini-Circuits XLF-252 shown in Figure 3.23 is a 3x3mm QFN low pass filter on the receive chain designed as a final filtering stage to remove higher frequency mixer RF and LO leakage prior to the signal passing to the ADC. The passband insertion loss is approximately 1 dB, and the 3 dB cutoff is at 3220 MHz, with 18 dB of rejection at the LO and RF frequencies. Performance is shown in Figure 3.24.

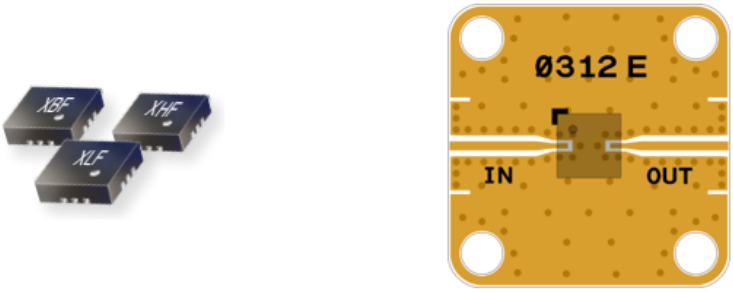

Figure 3.23: XLF-252 package [33] and X-Microwave layout [34].

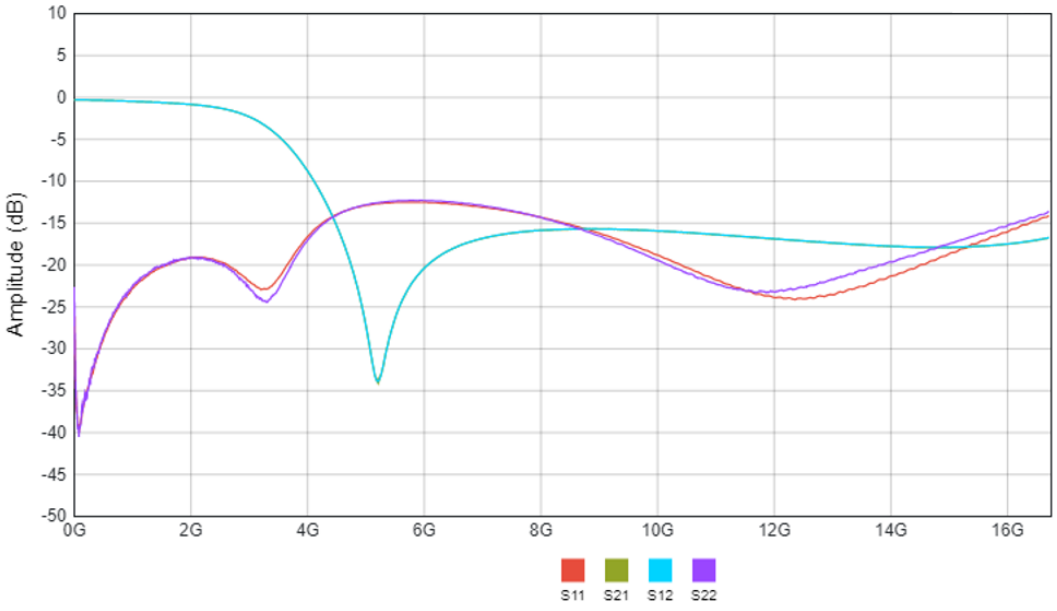

Figure 3.24: XLF-252 S-parameter performance [34].

XLF-133: LO Low Pass Filter

The Mini-Circuits XLF-133 shown in Figure 3.25 is a 3x3mm QFN low pass filter used to attenuate harmonic content from the local oscillator. The insertion loss at the LO frequency is approximately 2 dB, and the 3 dB cutoff is at 15.8 GHz. At twice the LO frequency, this filter has approximately 26 dB of rejection. Performance is shown in Figure 3.26.

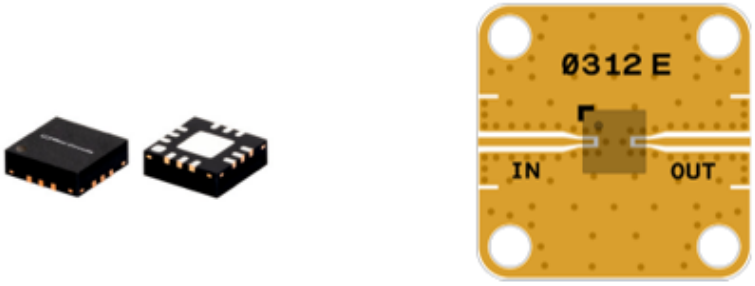

Figure 3.25: XLF-133 package [35] and X-Microwave layout [36].

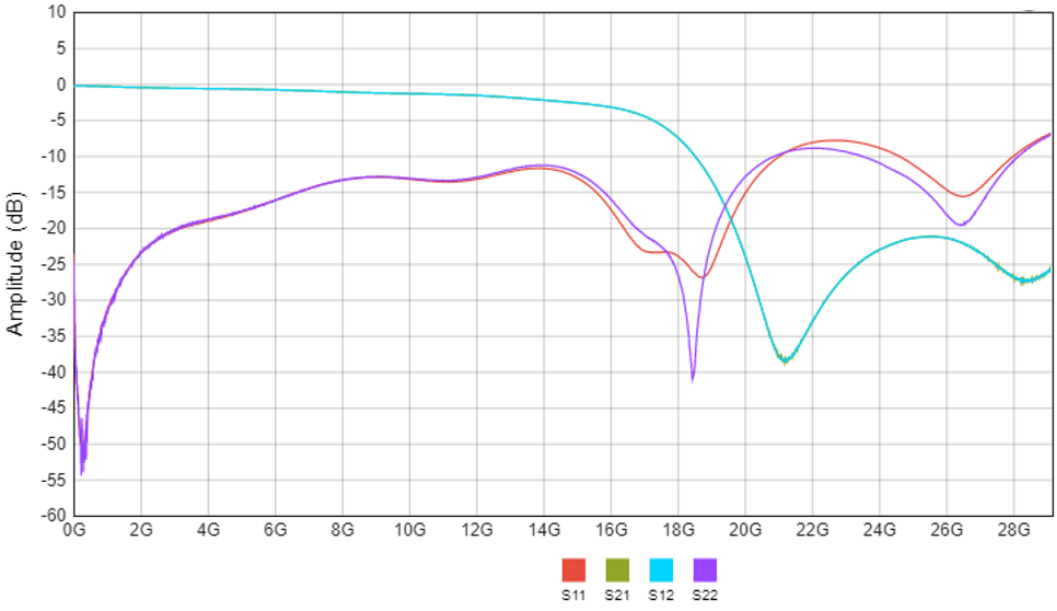

Figure 3.26: XLF-133 S-parameter performance [36].

FB-1300SM: LO Band Pass Filter

The Marki Microwave FB-1300SM shown in Figure 3.28 is a 8x25mm SMT band pass filter used to attenuate harmonic and subharmonic content from the local oscillator. The insertion loss at the LO frequency is approximately 2 dB, and the 3 dB bandwidth of 2730 MHz. At twice the LO frequency, this filter has approximately 30 dB of rejection. Performance is shown in Figure 3.28.

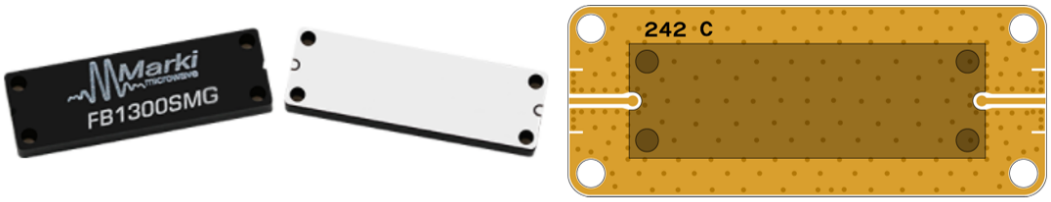

Figure 3.27: FB-1300SM package [37] and X-Microwave layout [38].

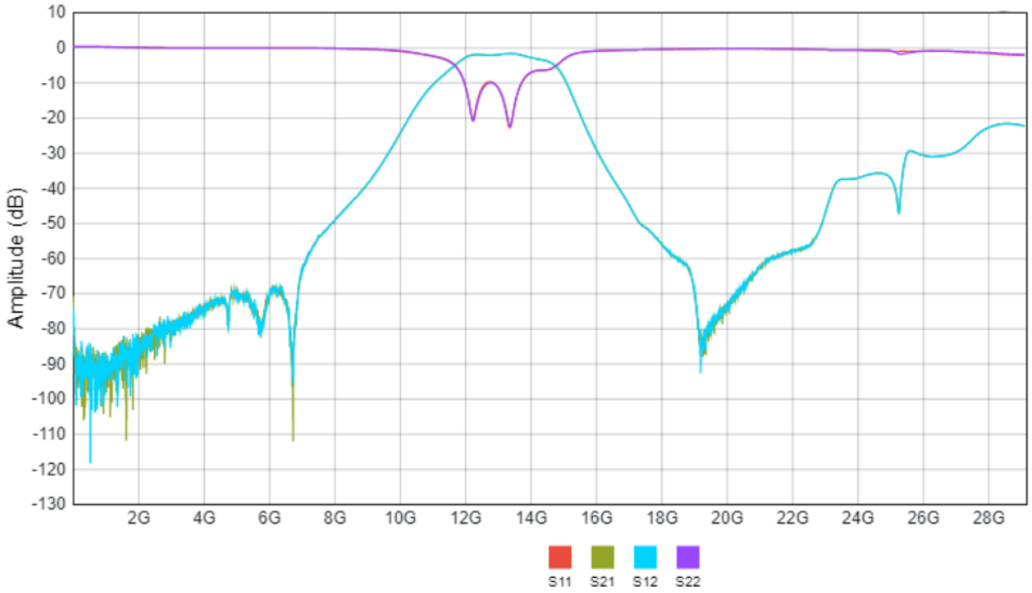

Figure 3.28: FB-1300SM S-parameter performance [38].

3.2 Digital Hardware

The primary focus of this work is on the RF/analog design of the system; however, the digital backend will be briefly discussed. The ARENA from Tomorrow.io (shown in Figure 3.29) is a highly integrated backend module with a software suite used to control the device.

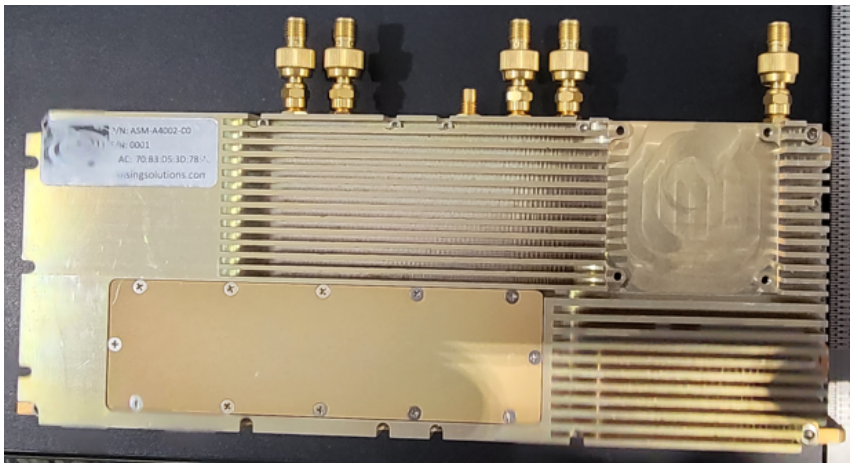

Figure 3.29: ARENA module.

The device requires a 6-30 V input supply and is controlled by an external laptop through an ethernet port. The ARENA has an integrated ADC (AD9689) to process receive data and DAC (AD9129) to generate transmit data. A user may interface with the module using a GUI through the manufacturer provided software. The overall module is a very simplified (for the end user) design which is highly configurable in software. The clock rates for the ADC and DAC are set to 1.6 GHz (provided by a synthesizer on the X-Microwave board), putting the IF in the third Nyquist zone.

The Analog Devices AD9129 is the 14-bit RF Digital-to-Analog Converter used to generate the 150 MHz wide linear-frequency-modulated (LFM) signal at the IF frequency centered at 2 GHz. The SFDR of the output is approximately in the

65 dBc range. This device is operated in it's proprietary "Mix-Mode", which allows carrier reconstruction in the second and third Nyquist zone. In this system, a CLK input of 1.6 GHz is fed to the device and the "Mix-Mode" is used to generate the 2 GHz centered IF in the third Nyquist zone.

The Analog Devices AD9689 is the 14-bit Analog-to-Digital Converter used to sample the received data after it passes through the downconversion stage of the front-end when receiving the signal. As discussed in the requirements section, the module is able to achieve 70 dBc of spurious free dynamic range with a maximum input power of +7 dBm and minimum input power of -52 dBm. This system is using a 1.6 GHz CLK input which places the 2 GHz IF in the third Nyquist band.

3.3 Power Supply

The overall system is powered by a 12 V "Super Start Platinum" truck battery. The 12 V is passed through a switching regulator (shown in Figure 3.30) to bring it to 10 V to pass into the X-Microwave system, which passes the 10 V into each bias controller to power the active RF devices. This 12 V is able to directly power the ARENA module and the ZVE-3W-183 high-power-amplifier.

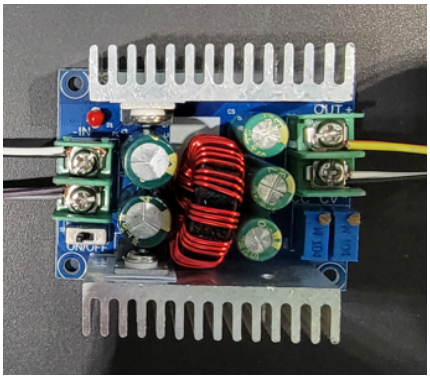

Figure 3.30: Power supply (switching regulator) for analog parts.

3.4 Cascade Analysis

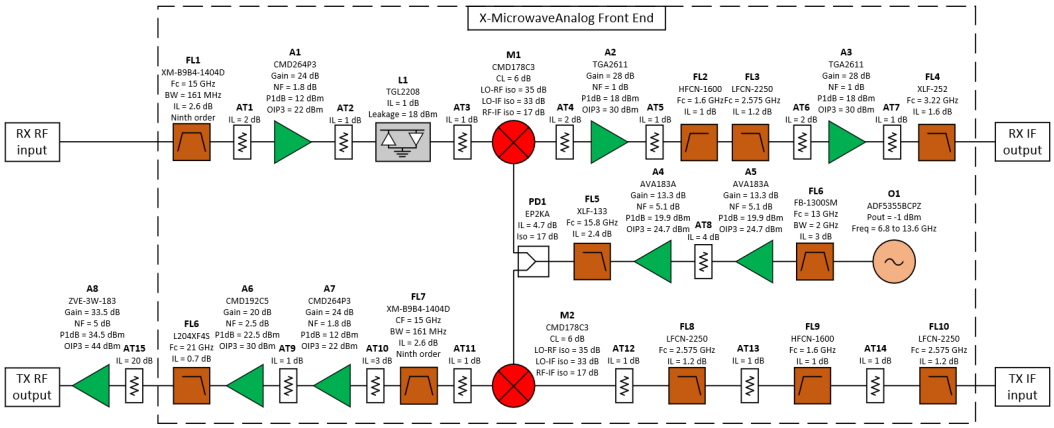

Figure 3.31: RF block diagram of front-end.

Now that the key components which will be used in the RF front-end have been discussed, the final design will be examined, starting with the RF block diagram of the X-Microwave system shown in Figure 3.31. Of note is that the limiter is after the first receive chain amplifier. This placement was chosen for the current experiment setup since the power level at the receiver LNA is anticipated to be very low even in worst case conditions of intended system operation. An attenuator has been inserted between the cavity filter and the first receive amplifier. This particular filter is very sensitive to impedance mismatches, which is solved using an attenuator. There is plenty of margin in the system noise figure, so this option was viable for the setup.

In this analysis, a few parameters of note will be calculated: signal power level throughout the design to ensure parts are operating in the linear region, gain in the TX and RX chains, receiver noise figure, and the spurious free dynamic range based on mixing products and expected harmonics. The cascade analysis will start with a block diagram analysis to prove out the design using datasheet values. The design will then be integrated into ADS to use S-parameter models for each part

on it's X-Microwave block to verify that performance of the actual parts when fully integrated will satisfy requirements. Linear models will be used for each component save for the mixers, which will use ADS mixer models. First, determine that the power level of the local oscillator generated by **O1** is at an acceptable level when it enters the LO port of the mixer. The conversion loss in the mixer for IF/RF and RF/IF conversion ranges between 5.5 dB to 6 dB within an LO drive range of +11 dBm to +15 dBm. The nominal output power of **O1** is -1 dBm. As shown in Figure 3.32, through the filtering, amplification and power splitting, the power level into the LO port ends up as +11.5 dBm, within acceptable ranges for **M1** and **M2**.

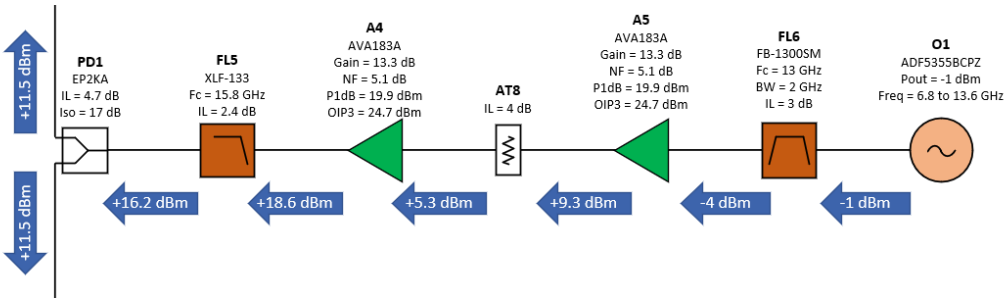

Figure 3.32: Signal analysis of local-oscillator signal path.

Now, verify that the X-Microwave block system will output a sufficiently high power level that it may be used to drive the transmit power amplifier. The measured output power of the ARENA DAC in was approximately -2 dBm. By the time the signal enters the mixer **M2**, the power level is -8.4 dBm, below the mixer's IP1dB of +9 dBm and IIP3 of +16 dBm with plenty of margin, so mixing products here should be very manageable since the system is operating in a more linear region. Proceeding through the TX RF stage, the signal exits the X-Microwave portion of the system at +21.5 dBm, more than enough to drive the power amplifier to produce a 2.5 Watt (34 dBm) output considering its 33.5 dB of gain. To achieve the desired output, the signal is reduced with 20 dB of attenuation prior to entering the power

amplifier and the output power is **+34.8 dBm** as shown in Figure 3.33.

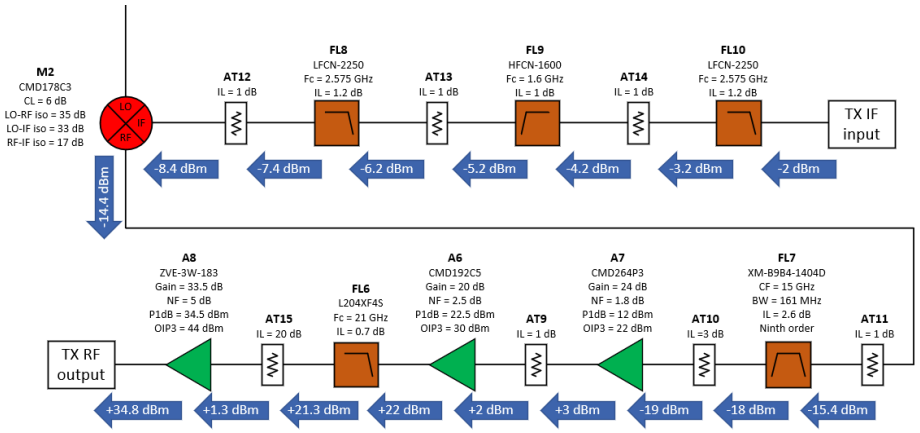

Figure 3.33: Signal analysis of transmit signal path.

Moving to the receive chain, start with the maximum expected input power level given previously as -72 dBm. After passing through the filtering and LNA, the signal is at -55.6 dBm as it reaches the RF port of the mixer **M1**, far below the mixer's IP1dB of +9 dBm and IIP3 of +16 dBm. After passing through the receive IF chain and entering the ADC, the signal is at approximately **-15.4 dBm** as shown in Figure 3.34, well within its dynamic range.

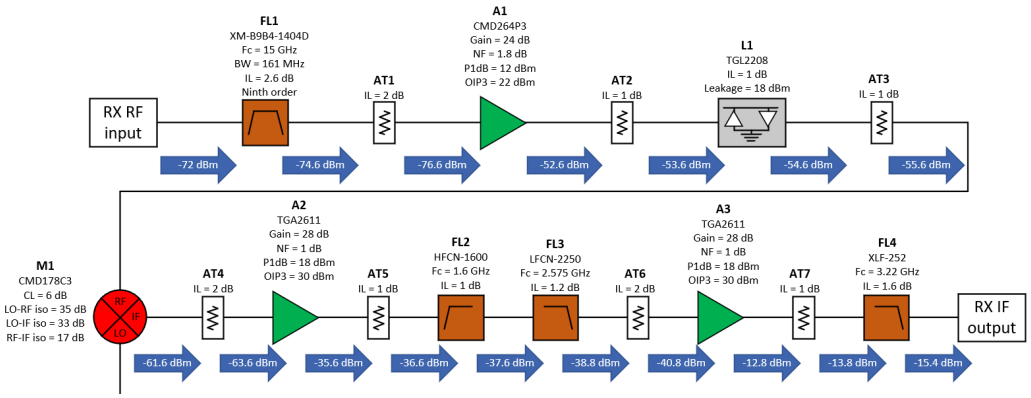

Figure 3.34: Signal analysis of receive signal path.

According to the analysis, the power levels in the front-end are at acceptable levels throughout the design and do not unintentionally saturate any of the active components when operating in a nominal condition. The transmit gain can now be extrapolated by taking the input vs output power level to get **+36.8 dB**, which exceeds the target minimum of +36 dB. The transmit amplifier is operating at the P1dB, however there is ample filtering on the receive chain and the antennas will provide some additional attenuation of harmonic content since it is outside of the band of operation. Calculating the gain similarly for the receive chain gets us **+56.6 dB**, which is safely within the bounds of the receiver gain requirements derived previously (41 dB to 88 dB).

The next system parameter calculated will be the noise figure. First, calculate the noise factor with (1.10). The noise figure is typically given for active components with gain, which can be converted directly to noise factor to be used in calculations. In passive components, noise figure is equal to the insertion loss of the component. Using datasheet values for the noise figures of each component, the final noise figure for the receive chain is approximately **6.6 dB**, which is under the 11.5 dB requirement with margin.

The last preliminary analysis to conduct by hand prior to simulations is intermodulation (IM) products from the mixer. The datasheet values for these products is shown in Figure 3.15. Calculating each frequency and passing it through filtering results in the mixing product levels shown in Figure 3.35.

RX IF Products (dBc)		nLO				
		0	1	2	3	4
mRF	0	-	63	81	> 90	> 90
	1	56	0	62	60	> 90
	2	92	76	119	> 90	> 90
	3	> 90	> 90	> 90	> 90	> 90
	4	> 90	> 90	> 90	> 90	> 90

Figure 3.35: Mixer product levels considering datasheet values, and passed through filtering.

The goal with these products is for each of them to be below the requirement of 70 dBc. There are 4 products that do not meet this through filtering alone: LO, RF, 2LO - RF, 3LO - RF. Each of these products are far enough outside of the operational band of the amplifiers to be suppressed an additional 20 dB minimum, putting them below the required SFDR.

3.5 Linear Simulations

Now that the preliminary cascade analysis has been conducted and system appears to meet requirements, the system will be simulated in ADS. First, a standard linear S-parameter simulation will be conducted to observe the linear performance over the band of operation. The linear performance through the cascaded system is examined to both verify that the system performance is within requirements, and to note any out-of-family results which may cause issues down the line, such as in key rejection points or the passband ripple

The nonlinear “Harmonic Balance” function of ADS allows us to simulate nonlinear system performance including mixers which produce intermodulation products. This function is able to integrate component performance using S-parameter

files seamlessly with the nonlinear models such as mixers to produce a result which will get close to what might be seen in actual hardware. For the S-parameter simulations, note the parameters shown in Table 3.1. These parameters were chosen to provide a sufficient simulation range to see all bands of operation and the second harmonic of the RF signal.

Table 3.1: S-Parameter Simulation Parameters.

Parameter	Value	Units	Description
f_{start}	1	GHz	Simulation start frequency
f_{stop}	32	GHz	Simulation stop frequency
f_{step}	1	MHz	Frequency step size
Z_1	50	Ω	Port 1 impedance
Z_2	50	Ω	Port 2 impedance

3.5.1 Transmit IF S-Parameter Performance

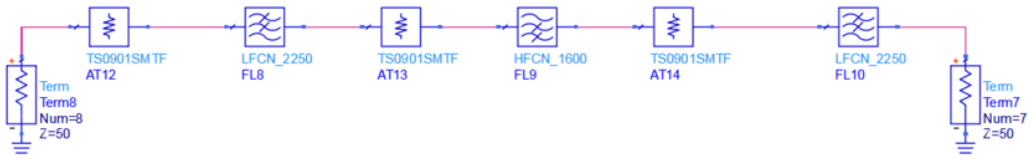

Figure 3.36: Transmit IF Chain in ADS - Signal flows right to left.

When examining the actual liner performance of these parts, consider the interaction of each part with its neighbor in the circuit. A component may not behave as expected when faced with a mismatched port. This is especially true for highly frequency selective parts such as filters (due to their performance fundamentally being dependent on how the signal energy propagates through capacitive or inductive impedances) or highly nonlinear parts such as mixers (due to signal reflections

re-entering the mixer port, creating more intermodulation products).

To begin, look at the linear performance of the transmit IF chain shown in Figure 3.36. This consists of filtering stages to remove harmonic and spurious content, and attenuators between each filtering stage to provide a good impedance match for the filters. The datasheet of the ADF5355 synthesizer, indicates a second harmonic level of -27 dBc and a third harmonic of -20 dBc. To reduce these harmonic levels below the -70 dBc requirement, there must be at least 50 dB of attenuation at the second harmonic (4 GHz) and 43 dB of attenuation at the third harmonic (6 GHz). Performance from the cascaded S-parameters indicates that the system is able to achieve approximately 60 dB of attenuation at 4 GHz and over 80 dB of rejection at the third harmonic, so the signal should be sufficiently clean to pass into the upconversion stage.

As shown in Figure 3.37, the gain is a nominal -4 dB and varies by approximately 0.7 dB across the band of operation. The minimum return loss in the passband is approximately 10 dB.

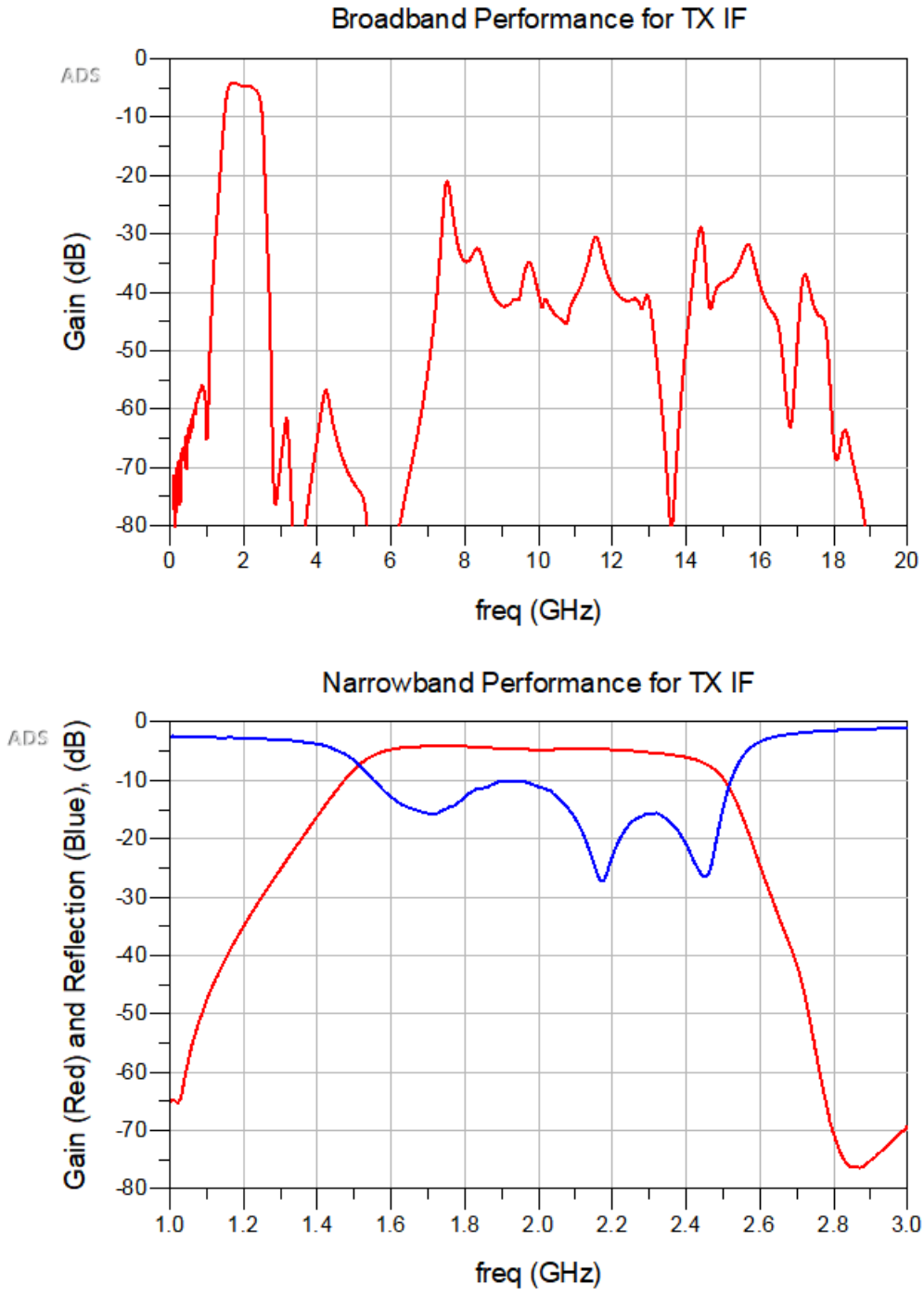

Figure 3.37: Transmit IF Chain Performance.

3.5.2 Transmit RF S-Parameter Performance

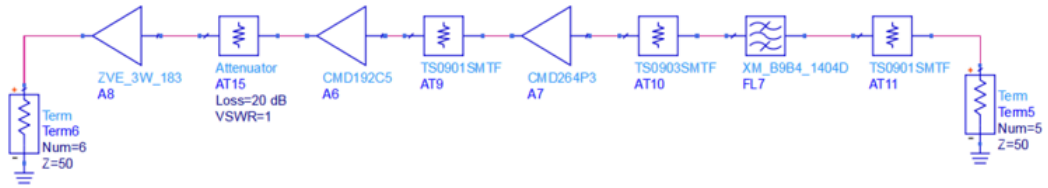

Figure 3.38: Transmit RF Chain in ADS - Signal flows right to left.

Moving on to the transmit RF section, the signal must be clean after passing through the mixer prior to reaching the antenna. The RF transmit stage is shown in Figure 3.38 and consists of a 9th order filter to reject any undesired intermodulation products from the mixer, an attenuator to provide a good impedance match between the mixer and the filter, two amplification stages to bring the signal up to a usable level for the final stage, attenuators between the amplifiers to tune the power level and reduce the chance of amplifiers entering a stage of positive feedback and oscillating due to the very high gain, and finally the transmit power amplifier.

Previously it was determined that the signal path selectivity was sufficient based on expected mixer product outputs. Outside of the passband there is 70+ dBc of rejection of all spectral content up to 35 GHz, so this still appears to hold true.

As shown in Figure 3.39, the gain is a nominal 47.7 dB and varies by approximately 2 dB across the band of operation. The return loss is 15 dB at a minimum in the band of operation.

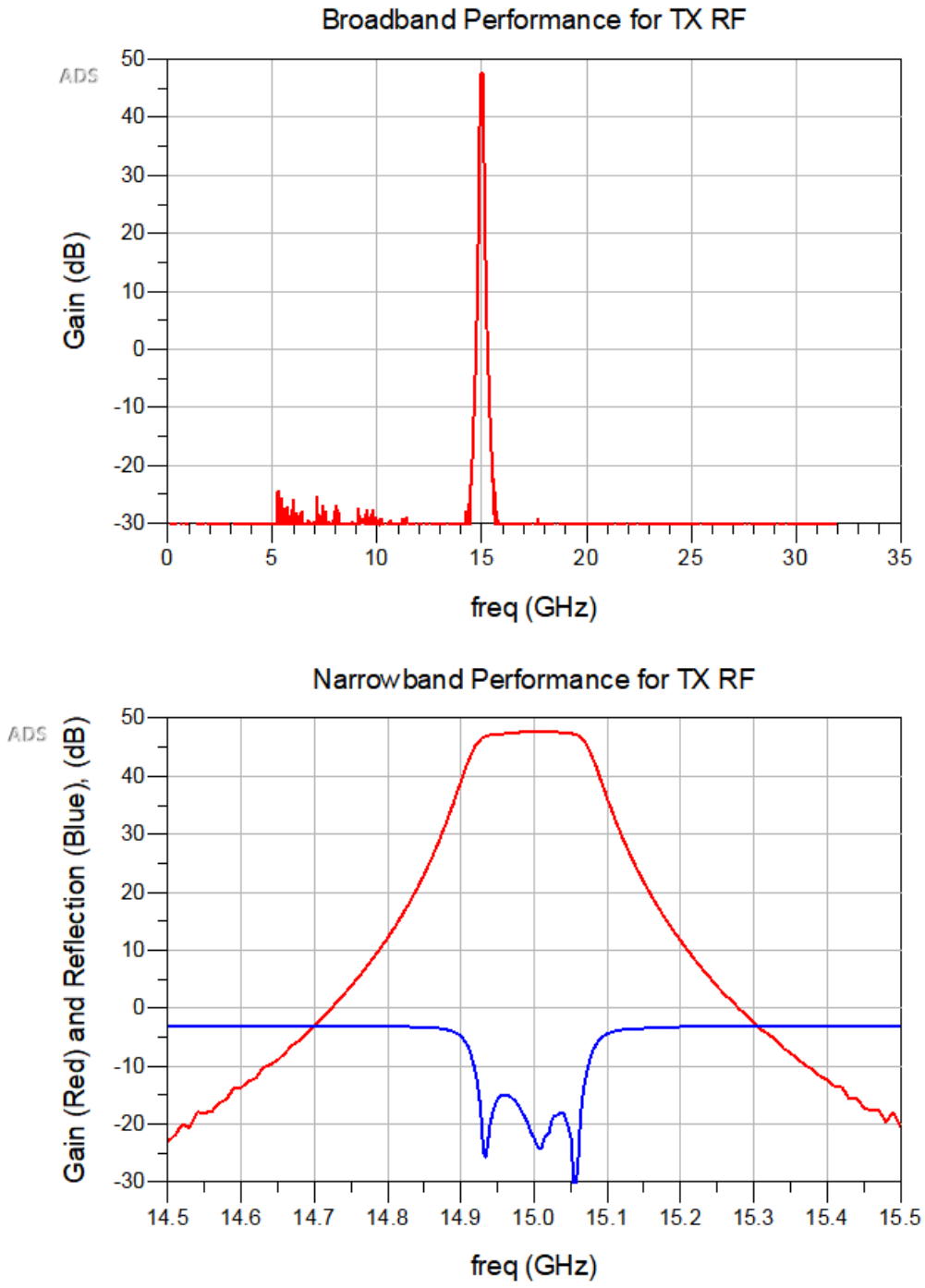

Figure 3.39: Transmit RF Chain Performance.

3.5.3 Receive RF S-Parameter Performance

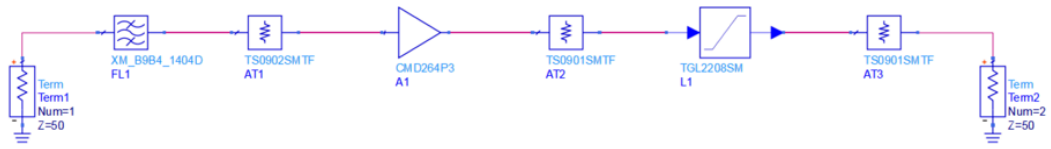

Figure 3.40: Receive RF Chain in ADS - Signal flows left to right.

The receive RF chain is shown in Figure 3.40 and consists of a 9th order band-pass filter to reject any undesired spectral content received from the antenna, an attenuator which was added to resolve a mismatch issue, a LNA to drive a relatively low noise figure, and a limiter whose purpose is to protect the ADC from railing. Attenuators flank the limiter to improve the impedance matching between components, especially with the mixer at the output of this chain.

Looking at the performance of the receive RF chain, the out of band rejection appears to be noise limited with the manufacturer provided S-parameters, however, a minimum of 65 dBc of rejection is achievable. The system would also not be receiving any appreciable signals transmitted from the system in the regions which are noise limited (5 to 10 GHz), therefore this does not appear to be a concern for system performance.

As shown in Figure 3.43, the gain is a nominal 15.5 dB and varies by approximately 3 dB across the band of operation. The return loss is a minimum of approximately 14 dB in the band of operation.

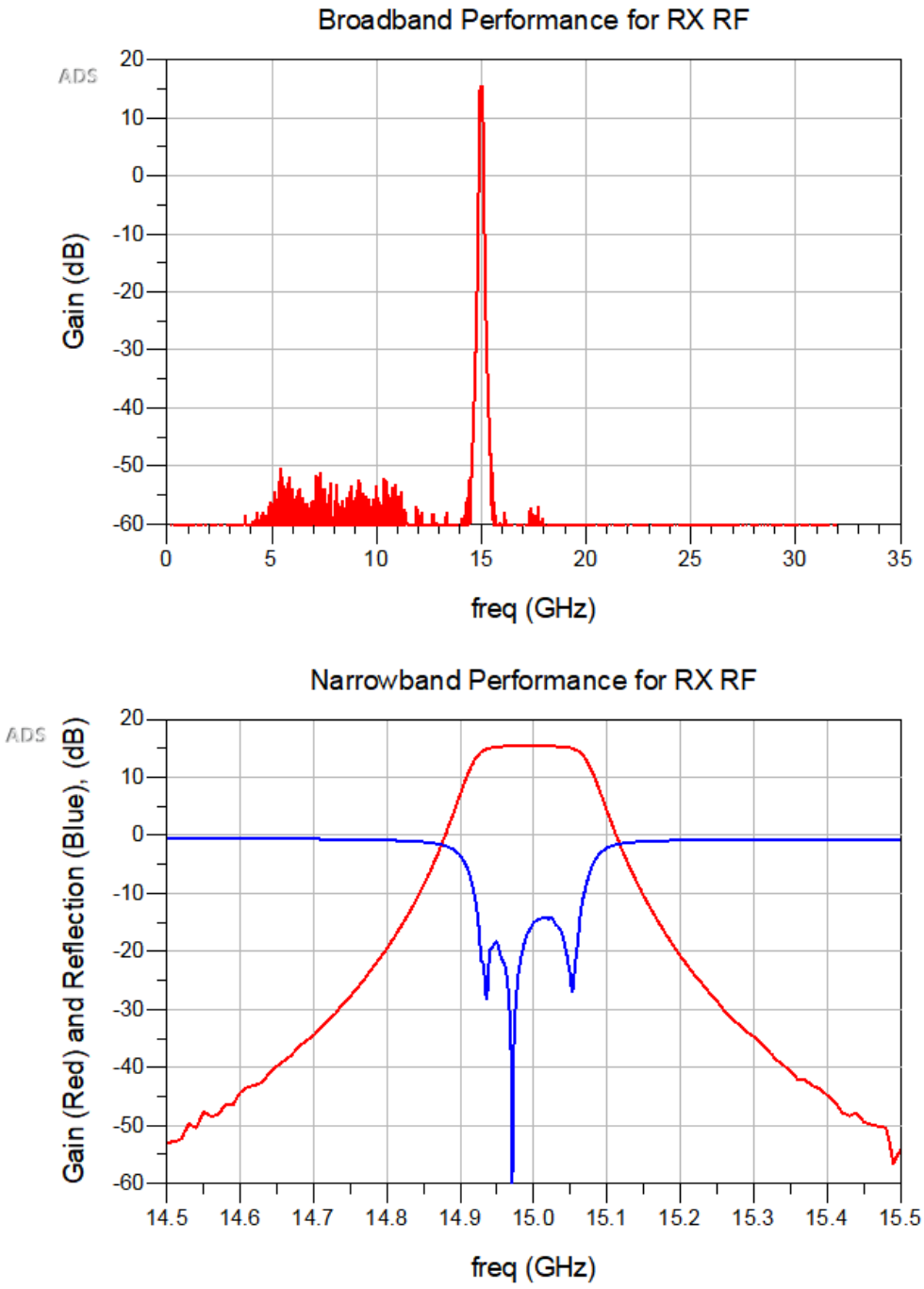

Figure 3.41: Receive RF Chain Performance.

3.5.4 Receive IF S-Parameter Performance

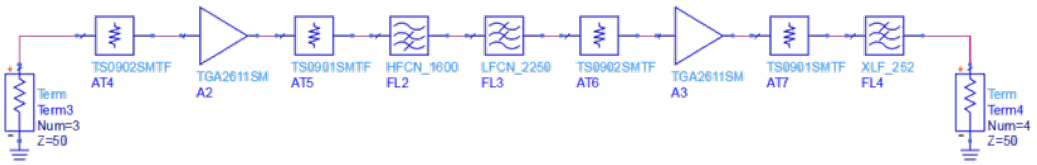

Figure 3.42: Receive IF Chain in ADS - Signal flows left to right.

Finally, the receiver IF chain is shown in Figure 3.42 and consists of a series of attenuators between components to impedance match where needed, amplifiers as a gain block, and filters to remove undesired mixer products. The first goal is for the filtering to reject and undesired intermodulation products. Figure 3.43 shows that any spectral content near the RF or LO frequencies is rejected 80+ dB by the filtering.

Now, higher order products resulting from the downconversion will be examined. Of particular note based on the S-parameter performance is a second harmonic of IF at 4 GHz, which is also the same frequency as the 4th order product 2RF - 2LO. From the mixer datasheet, this product is expected to be at 64 dBc, which when compounded with the 45 dB of rejection from filtering becomes well within an acceptable range.

The gain is a nominal 49.5 dB and varies approximately 0.3 dB across the band of operation. The return loss is approximately 14 dB in the band of operation.

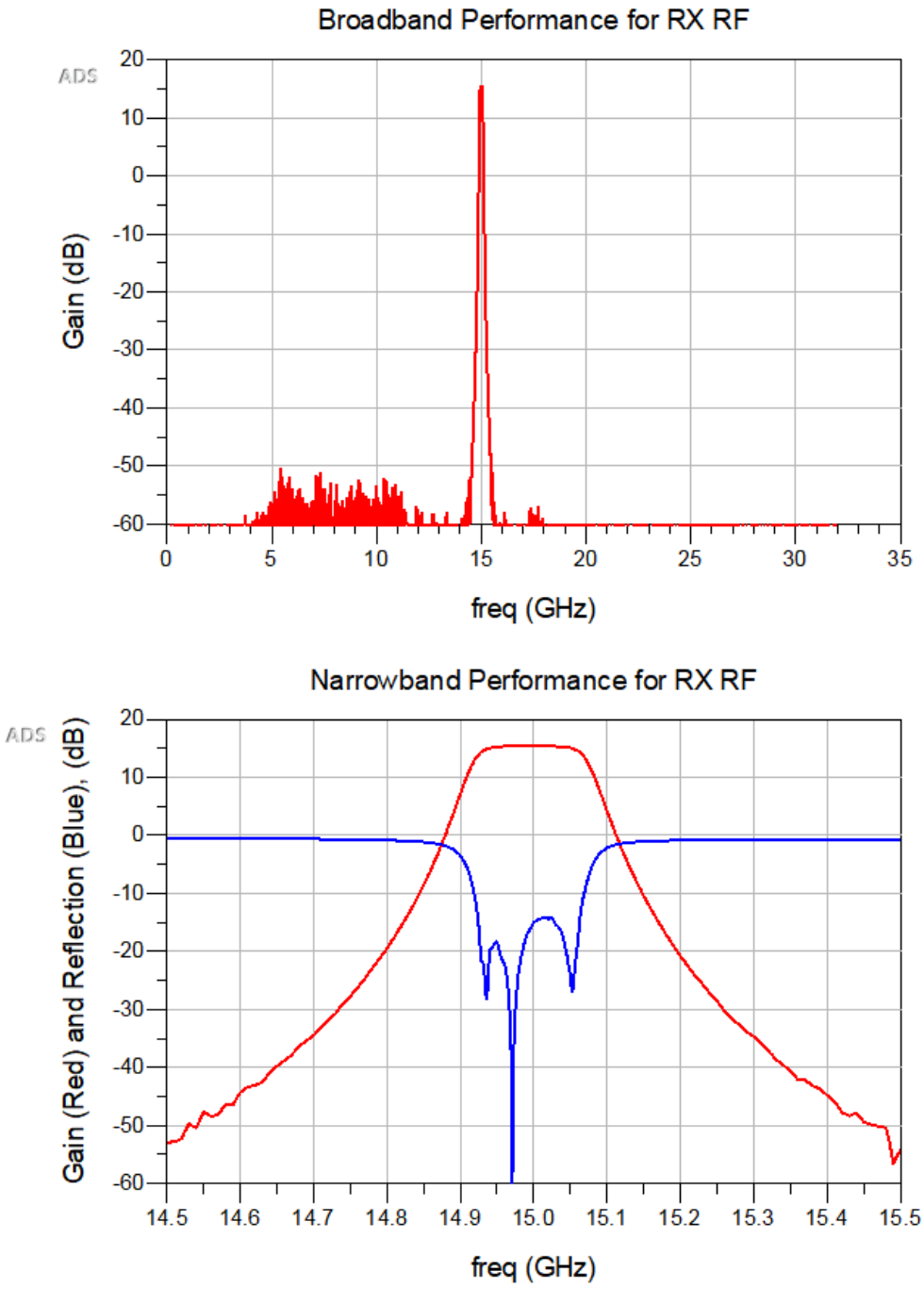

Figure 3.43: Receive RF Chain Performance.

3.6 Non-linear Simulations

Now that the linear performance of the system has been examined in segments via S-parameters, those models will be integrated into a Harmonic Balance simulation. This simulation applies the S-parameter models of each component to input frequencies and higher order products of those input frequencies propagating through the circuit. The band of interest will be examined along with any intermodulation products that are visible within the SFDR requirement.

There is currently no non-linear model available for the CMD178C3 so the "Mixer2" model from ADS will be used, incorporating datasheet parameters to achieve the highest degree of accuracy possible with this simulation setup. The IF is swept from 1.925 GHz to 2.075 GHz in 10 MHz steps to observe the nonlinear performance through the system. Similarly, the RF is swept from 14.925 GHz to 15.075 GHz.

The oscillator power level is set at -1 dBm per the datasheet values previously discussed. Commensurate with lab measurements, the TX IF input from the synthesizer is set at -2 dBm. Received signal power will be set at -72 dBm to examine the worst-case nonlinear performance when the input power is at the maximum expected power level. The ADS schematic and simulation setup is shown in Figure 3.44.

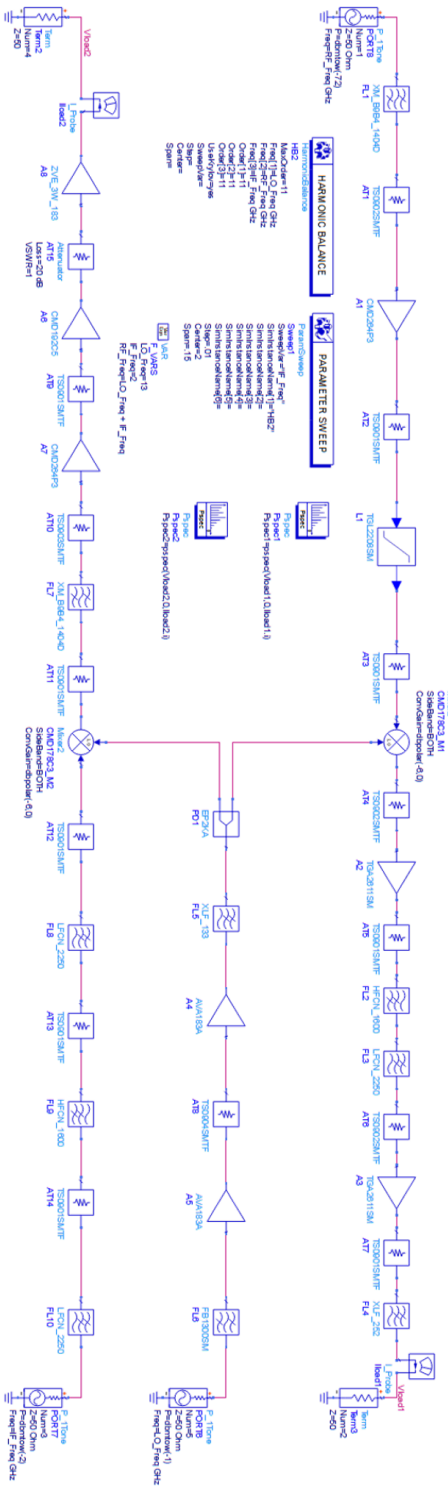

Figure 3.44: Front-end Harmonic Balance Model.

Table 3.2: Harmonic Balance Simulation Parameters.

Parameter	Value	Units	Description
$P_{TX,IF}$	-2	dBm	Input transmit IF power level
$P_{RX,RF}$	-72	dBm	Input receive RF power level
f_{LO}	13	GHz	LO frequency tone
f_{RF}	15	GHz	RF center frequency
f_{IF}	2	GHz	IF center frequency
f_{span}	150	MHz	Frequency span (signal bandwidth)
n	15	–	Number of frequency points
$MaxOrder$	11	–	Maximum order of nonlinear products

The harmonic balance simulation was set up with the conditions shown in Table 3.2. Under these conditions, the output spectrum is observed at the transmit RF port in Figure 3.45. From the broadband spectrum, there is no substantial spurious content at the output of the transmit amplifier. There is some minor LO leakage, however this is approximately 80 dBc, and therefore meets the SFDR requirements. The narrowband spectrum shows a nominal power output of 35 dBm (3.16 W) with approximately 3 dB of gain variation over the band of operation. The numbers from these simulations matches the cascade analysis to approximately 0.2 dB.

The transmit RF is operating near compression (the non-linear region of operation) for the driver amplifier (A6) and power amplifier (A8), so nonlinear characteristics will be simulated for these components.

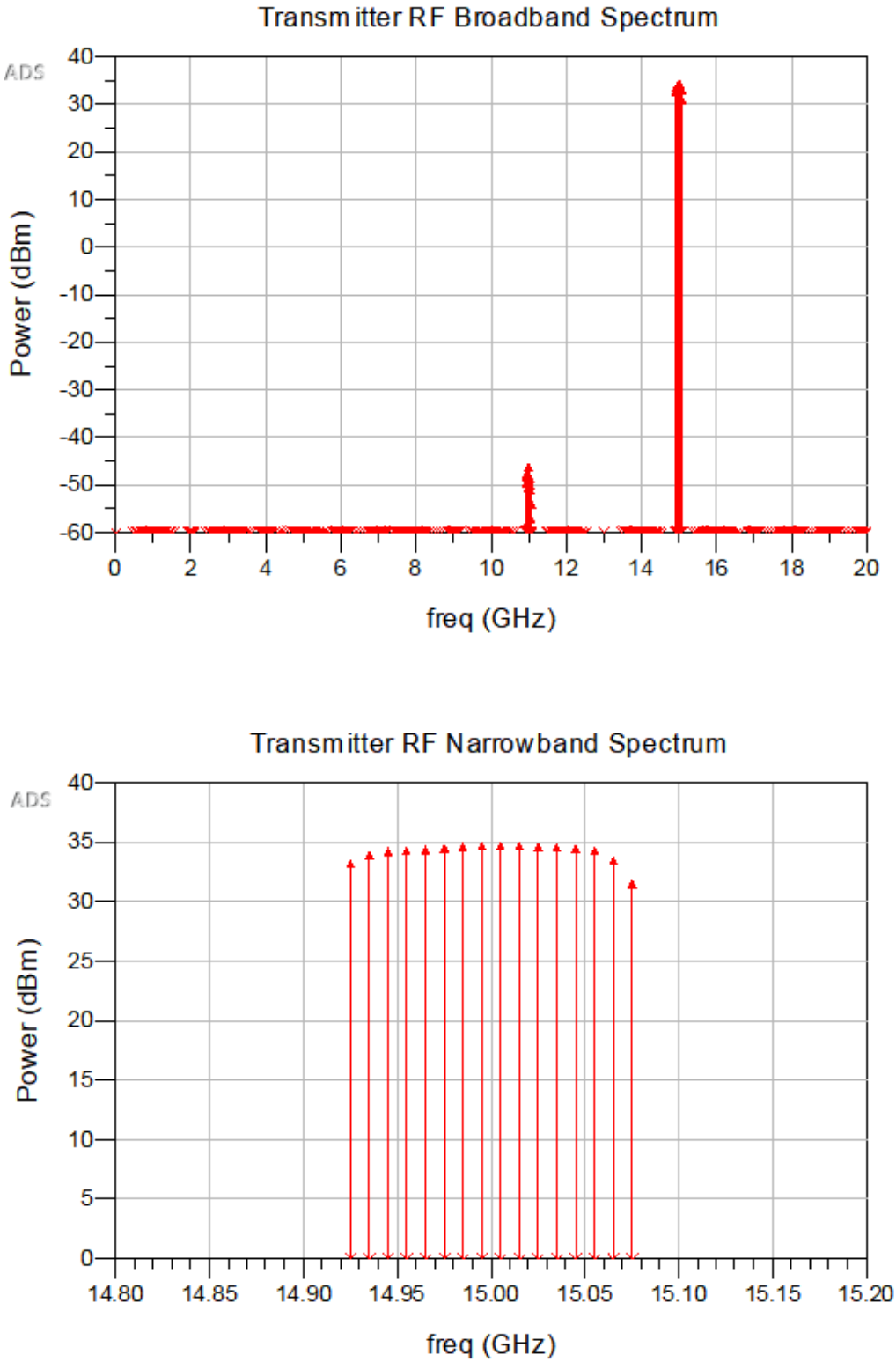

Figure 3.45: TX RF output spectrum using liner component for all components other than mixers.

The RX IF spectrum was integrated into this simulation and can be seen in Figure 3.46. The broadband spectrum plot indicates that there is no spectral content down to 80+ dBc from the downconversion that is able to pass through the IF chain. The narrowband plot shows the nominal power level to be approximately -13.3 dBm with approximately 3 dB of variation in the band of operation. These numbers are approximately 2 dB higher than what was calculated in the cascade analysis, which is well within an acceptable range as defined by the gain requirement. The signal level here is low enough that no components simulated with linear models are operating close to a non-linear region, so no additional analysis is required.

The LO power level entering each mixer following the power splitter will also be examined to verify sufficient LO drive. It is desirable to achieve an LO signal level as close as possible to the datasheet test conditions so that the other parameters from the datasheet will be accurate, as each parameter is given based on a specific LO drive. The LO level in the harmonic balance simulation is approximately +13.5 dBm, which is 2 dB higher than indicated by the cascade analysis, but is very close to test condition power level from the datasheet (+13 dBm).

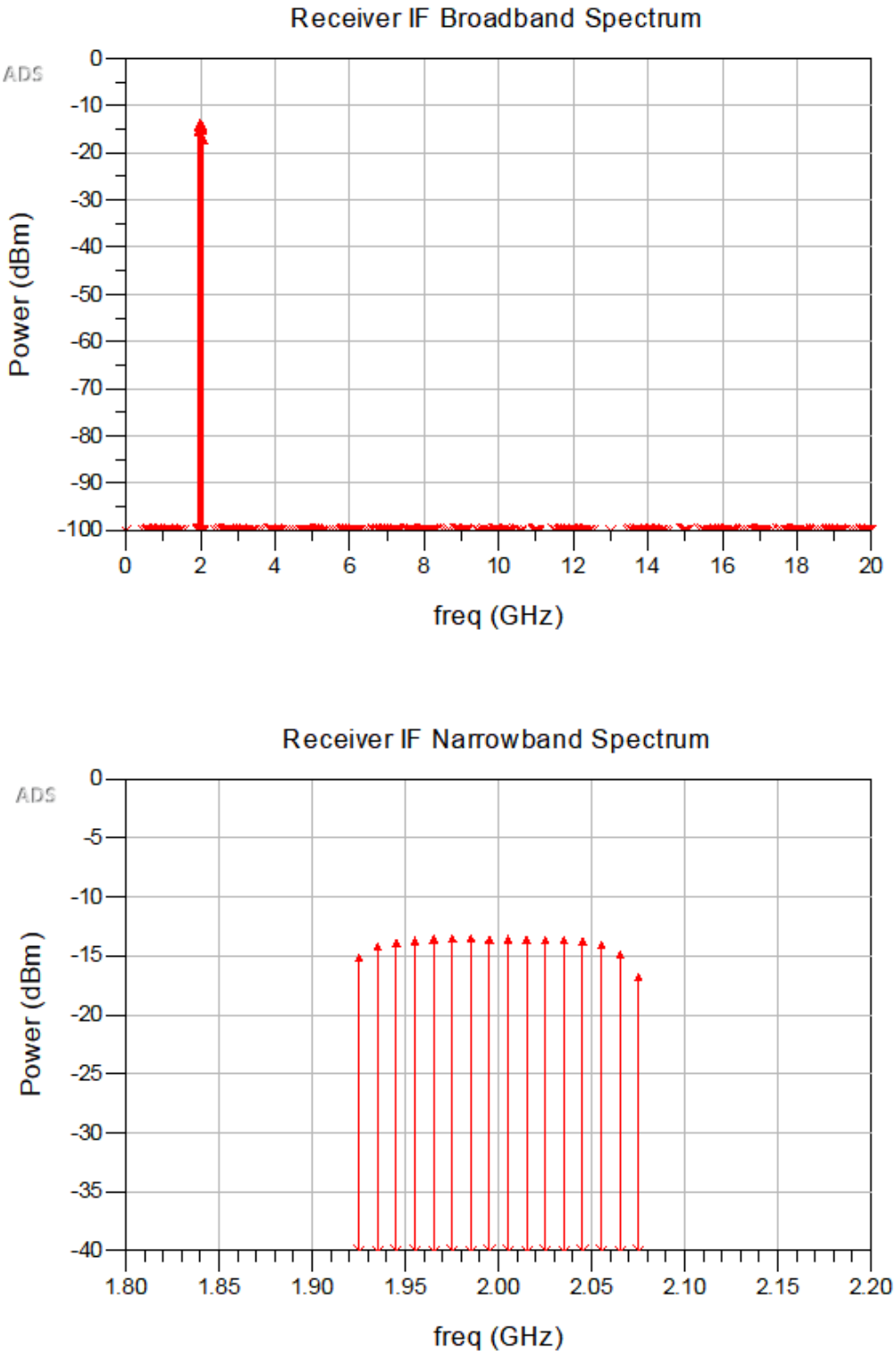

Figure 3.46: RX IF output spectrum using liner component for all components other than mixers.

As previously discussed, amplifiers operating in or near the nonlinear region may have undesired harmonics. If an amplifier is indeed operating within a few decibels of its P1dB point, an additional simulation will be ran with an ADS non-linear amplifier model in its place and examine the spectral content.

The amplifiers **A6** and **A8** are operating in a non-linear region, so they are replaced with models which integrate these characteristics, as shown in Figure 3.47. Running the simulation again results in a very similar output (shown in Figure 3.48) compared to using simple linear models, so it appears there are no substantial concerns with the non-linear behavior of the amplifiers which present themselves here. Looking further out to the second harmonic area around 30 GHz is necessary to verify that harmonic content generated by operating in the non-linear region is not substantial enough to risk violating system requirements. The nominal output power is slightly lower at +34.3 dBm with a gain variation of 1.3 dB across the band of operation.

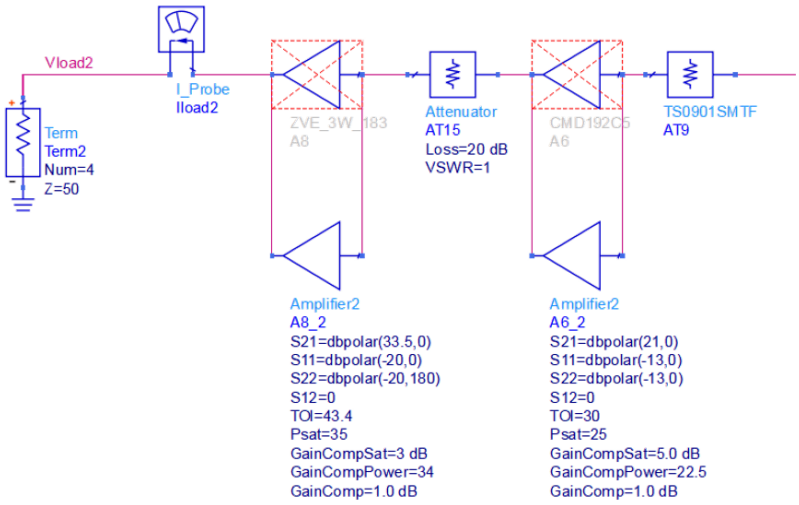

Figure 3.47: Replacing linear S-parameter models with non-linear counterparts.

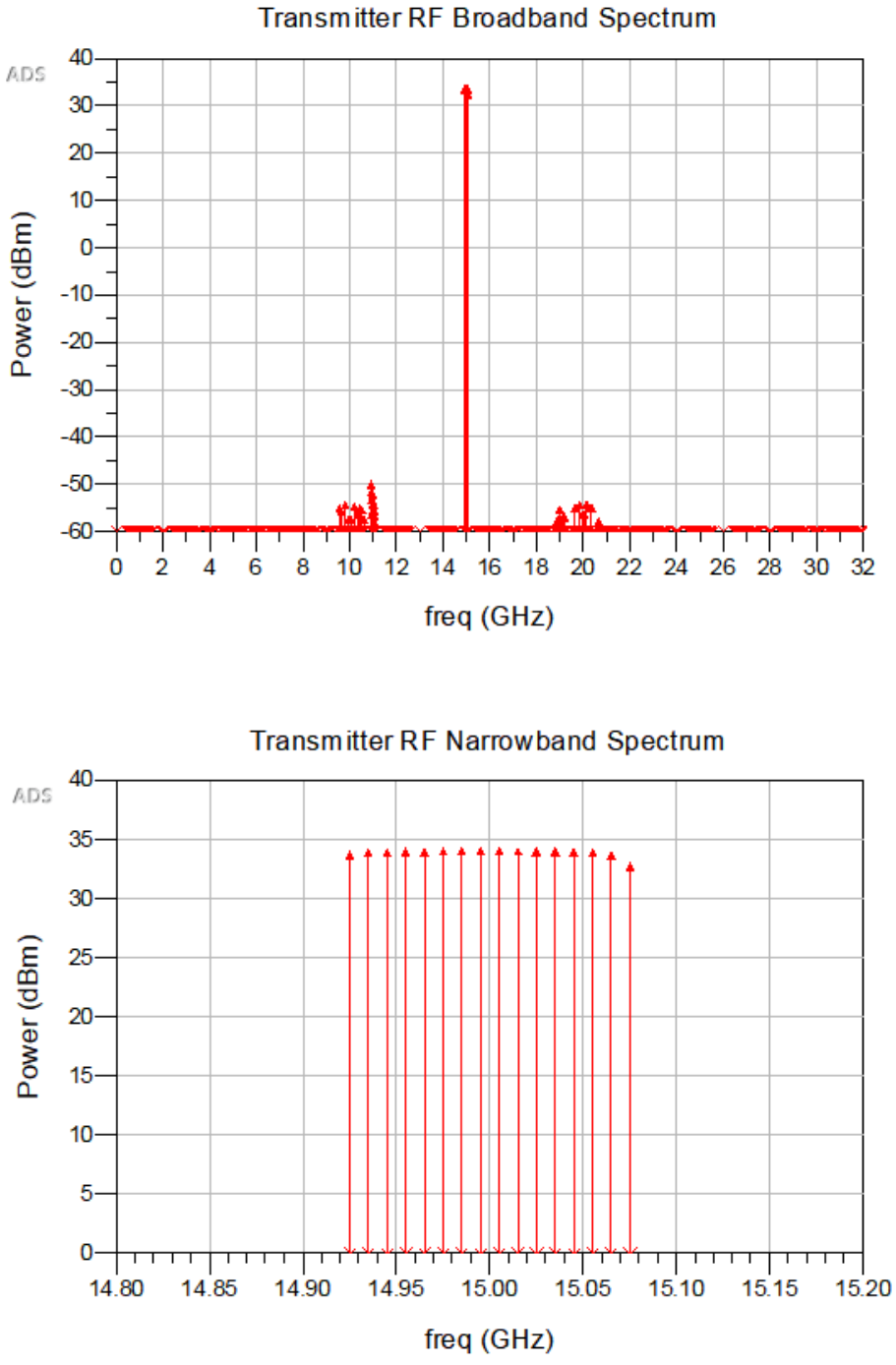

Figure 3.48: ADS simulation of TX RF output using non-linear models.

3.6.1 Prototype System

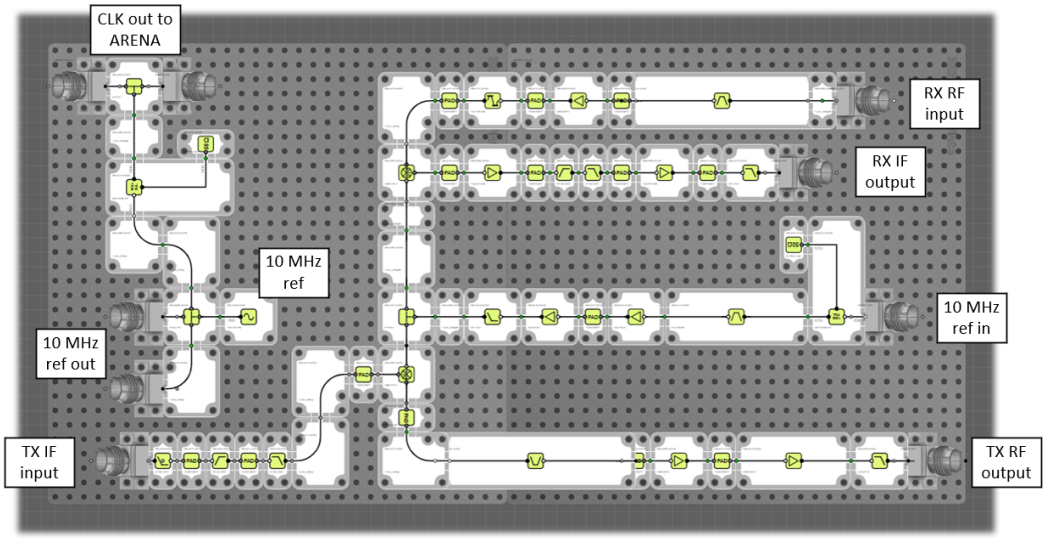

Figure 3.49: X-Microwave Hardware Block Diagram.

Now that there is a baseline for expected performance, the hardware block diagram as realized in the X-Microwave layout tool is designed, shown in Figure 3.49. For this design, the flow of the RF circuitry follows what was simulated previously. A 10 MHz reference signal is included for coherency between the ARENA backend module and the LO (and by extension, RF and IF) signal. This reference also drives the clock generating synthesizer which provides the clock that is passed to the ARENA.

The bill of materials (BOM) for the system is based on the X-Microwave design and is shown in Table 3.3. This BOM covers the RF hardware, its supporting electronics, and the backend module. The RF hardware comes out to approximately $19,700, which includes all of the components discussed previously, in addition to the chassis, shielding, transmission line, and other misc design components. The ARENA was approximately $24,000, as it is a highly integrated module which pro-

vides capability beyond the direct needs of this project. The total cost of the system (excluding peripherals such as laptops or SAR specific IMU hardware) comes out to $43,730.90.

Table 3.3: Radar Bill of Materials.

X-Microwave P/N	Category	QTY	Manufacturer	ManufacturerP/N	Each Price	Total Price
XM-PB1-292F	Housing	9	X-Microwave	XM-PB1-292F	$239.95	$2,159.55
XM-PP2-3232-01	Housing	3	X-Microwave	XM-PP2-3232-01	$299.95	$899.85
XM-LS1-0404	Housing	11	X-Microwave	XM-LS1-0404	$16.95	$186.45
XM-WT1-0501	Housing	11	X-Microwave	XM-WT1-0501	$16.95	$186.45
XM-WT1-0401	Housing	35	X-Microwave	XM-WT1-0401	$16.95	$593.25
XM-LS1-0204	Housing	13	X-Microwave	XM-LS1-0204	$16.95	$220.35
XM-LS1-0304	Housing	9	X-Microwave	XM-LS1-0304	$16.95	$152.55
XM-WT1-0601	Housing	97	X-Microwave	XM-WT1-0601	$16.95	$1,644.15
XM-A7J3-0404D	Oscillator	1	Connor-Winfield	TB602-050.0M	$175.00	$175.00
XM-A7T8-0404D	Active Bias Controller	1	ADI	ADP7142ACPZN-R7	$150.00	$150.00
XM-ANCHOR2	Housing	111	X-Microwave	XM-ANCHOR2	$9.95	$1,104.45
XM-A1M4-0404D	Splitter	1	Mini-Circuits	SCN-3-13+	$65.00	$65.00
XM-ANCHOR2-A(L)	Housing	9	X-Microwave	XM-ANCHOR2-A(L)	$9.95	$89.55
XM-ANCHOR2-A(R)	Housing	9	X-Microwave	XM-ANCHOR2-A(R)	$9.95	$89.55
XM-A321-0405D	T-Line	2	X-Microwave	XM-A321-0405D	$14.00	$28.00
XM-GSGJ	Housing	67	X-Microwave	XM-GSGJ	$4.00	$268.00
XM-ANCHOR2-AA	Housing	5	X-Microwave	XM-ANCHOR2-AA	$9.95	$49.75
XM-A2M5-0204D	T-Line	3	X-Microwave	XM-A2M5-0204D	$12.00	$36.00
XM-A3R9-0409D	Active Bias Controller	2	ADI	ADP7142ACPZN	$195.00	$390.00
XM-A741-0409D	PLL-VCO	2	ADI	ADF5355BCPZ	$195.00	$390.00
XM-LS1-0804	Housing	21	X-Microwave	XM-LS1-0804	$16.95	$355.95
XM-WT1-0301	Housing	33	X-Microwave	XM-WT1-0301	$16.95	$559.35
XM-A354-0204D	Load	2	X-Microwave	50 Ohm Load	$45.00	$90.00
XM-A2M6-0304D	T-Line	1	X-Microwave	T-Line_Straight	$12.00	$12.00
XM-LT1-0204	Housing	5	X-Microwave	XM-LT1-0204	$16.95	$84.75
XM-A2M8-0404D	T-Line	6	X-Microwave	T-Line_90deg	$14.00	$84.00
XM-A1K5-0404D	Splitter	1	Mini-Circuits	GP2S1+	$65.00	$65.00
XM-A319-0405D	T-Line	2	X-Microwave	T-Line_90deg	$14.00	$28.00
XM-C756-0808D	Band Pass Filter	1	Mini-Circuits	CBP-1034C+	$125.00	$125.00
XM-A2J9-0404D	Voltage Regulator	4	TI	LP38798SD	$65.00	$260.00
XM-A8B2-0404D	Amplifier	2	Mini-Circuits	GVA-62+	$84.00	$168.00
XM-A217-0204D	Attenuator	10	EMC	TS0901SMTF	$78.00	$780.00
XM-A774-0404D	Limiter	1	Qorvo	TGL2208-SM	$150.00	$150.00
XM-A2R9-0404D	Voltage Regulator	2	TI	LP38798SD	$65.00	$130.00
XM-A9W8-0404D	Amplifier	2	Custom MMIC	CMD264P3	$125.00	$250.00
XM-A218-0204D	Attenuator	6	EMC	TS0902SMTF	$78.00	$468.00
XM-B9B4-1404D	Band Pass Filter	2	X-Microwave	BPC18258-feet	$500.00	$1,000.00
XM-B7Y1-0204D	Low Pass Filter	1	Mini-Circuits	LFCV-1450+	$48.00	$48.00
XM-A4D1-0604D	Multiplier	2	MACOM	SFD25	$300.00	$600.00
XM-A5B6-0404D	Mixer	2	Custom MMIC	CMD178C3	$150.00	$300.00
XM-B1M9-0404D	Amplifier	3	Qorvo	TGA2611-SM	$275.00	$825.00
XM-B1N1-0404D	Active Bias Controller	3	TI	LT3045EDD#TRPBF	$150.00	$450.00
XM-A1D3-0204D	High Pass Filter	2	Mini-Circuits	HFCN-1600+	$45.00	$90.00
XM-A1A5-0204D	Low Pass Filter	3	Mini-Circuits	LFCN-2250+	$45.00	$135.00
XM-A3F8-0404D	Low Pass Filter	1	Mini-Circuits	XLF-252+	$51.00	$51.00
XM-A2M7-0404D	T-Line	1	-	T-Line_Straight	$14.00	$14.00
XM-C357-0404D	Splitter	1	Mini-Circuits	EP2KA+	$150.00	$150.00
XM-A3G9-0404D	Low Pass Filter	1	Mini-Circuits	XLF-133+	$52.00	$52.00
XM-B216-0404D	Amplifier	2	Mini-Circuits	AVA-183A+	$95.00	$190.00
XM-A7J1-1004D	Band Pass Filter	1	Marki	FB-1300SM	$185.00	$185.00
XM-A192-0204D	Low Pass Filter	1	Mini-Circuits	LFCN-530+	$46.00	$46.00
XM-A219-0204D	Attenuator	1	EMC	TS0903SMTF	$78.00	$78.00
XM-A379-0804D	Active Bias Controller	1	ADI	HMC980LP4E	$195.00	$195.00
XM-A3E6-0804D	Amplifier	1	Custom MMIC	CMD192C5	$265.00	$265.00
XM-A2B8-0404D	Low Pass Filter	1	DLI	L204XF4S	$144.00	$144.00
ZVE-3W-183	High Power Amplifier	1	Mini-Circuits	ZVE-3W-183	$1,424.95	$1,424.95
ARENA	Backend module	1	Remote Sensing Solutions	ARENA		$24,000.00
-	Misc cabling & hardware	1	Mini-Circuits	-		$1,000.00
				TOTAL		**$43,730.90**

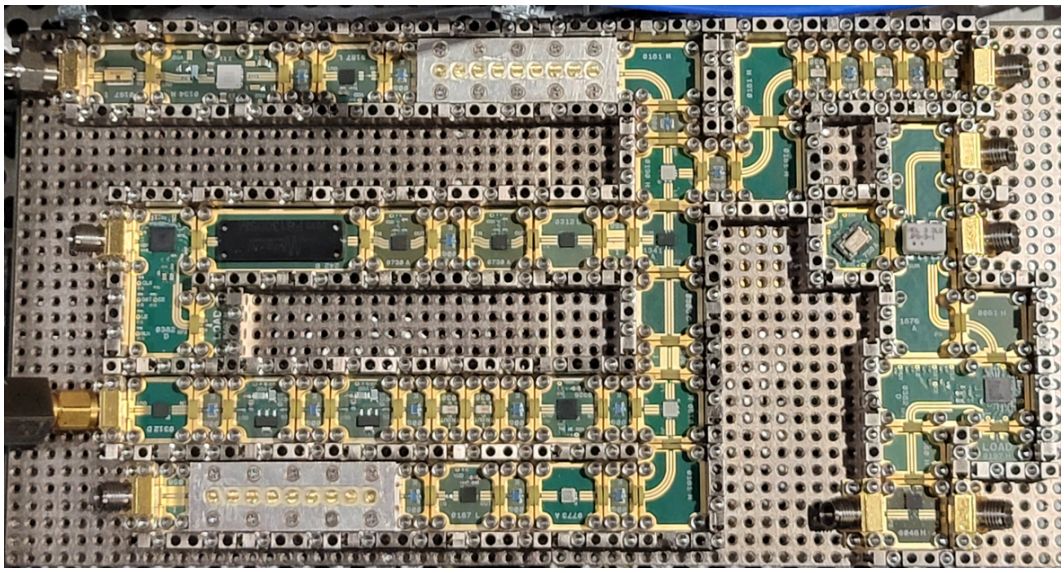

Figure 3.50: Assembled X-Microwave RF Circuitry.

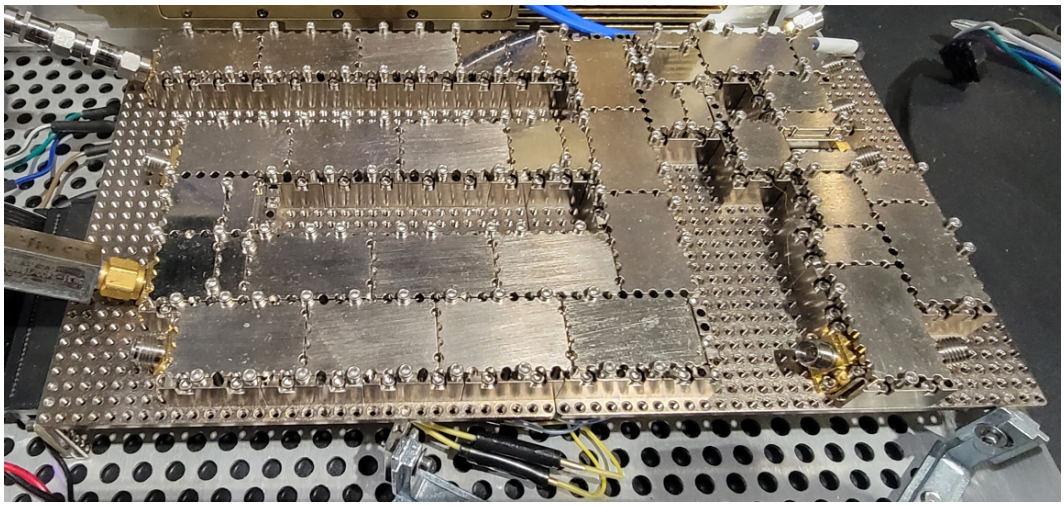

Figure 3.51: Assembled X-Microwave RF Circuitry with Shielding.

The system was assembled and the result is shown in Figure 3.50 (unshielded) and Figure 3.51 (shielded). Note that the biasing boards for all of the active parts are on the backside of the plate. Shielding was integrated to prevent coupling between signal paths and prevent cascaded amplifiers from creating a positive feedback loop, causing oscillation. After the radar was assembled, it was taken out for test.

Chapter 4

Synthetic Aperture Radar Testing and Results

In this chapter, the radar system designed in the previous chapter will be utilized and the results will be evaluated. Basic SAR processing for a typical use case will be discussed first. Then the test setup will be discussed, including the inertial measurement unit and GPS sync setup. Finally results from conducting a ground test and flight tests will be examined, including the 30 degree look angle application with its associated SAR image, and a Vertical SAR (VSAR) application with its associated image - used as an elevation profile.

4.1 SAR Processing

A SAR's primary defining characteristic is that it uses a number of radar pulses directed at the target scene over the course of a flight path to create a much larger aperture than would be possible with a physical antenna. The distance traveled over the course of the CPI effectively acts as the "synthetic aperture" of the radar, defining azimuth (along-track) a synthetic aperture length of

$$L = \frac{R_0 \lambda}{2\rho_a sin\theta_g} < \frac{R_0 \lambda}{l} \tag{4.1}$$

where R_0 is the range, λ is the carrier wavelength, ρ_a is the azimuth resolution, θ_g is the grazing angle, and l is the physical antenna aperture length in azimuth [39].

SAR processing is essentially a matched filter for each pixel. The filter is applied to each frequency sample and each pulse to create an array of scattering estimates mapping to each pixel, forming the image. Considering a radar that collects L_{ADC} samples per pulse in fast-time and find the length K FFT (such that $K > L_{ADC}$), the receive signal is

$$X_r(F_k, m) = \alpha X_p(F_k) e^{-j2\pi F_0 \tau_m} e^{-j2\pi F_k \tau_m} \tag{4.2}$$

where α is the scaling factor, m is the pulse number, τ is the propagation delay, F_0 is the carrier frequency, and the range-frequencies are defined as $F_k = -0.5F_s + k\frac{F_s}{K}$, where $k = 0, 1, 2, ..., K-1$ and F_s is the ADC sampling rate. Applying a single pulse matched-filter to this received signal results in

$$\begin{aligned} y_p(t, m) &= \int_{-\infty}^{\infty} X_r(F, m) X_p^*(F) e^{j2\pi F t} dF \\ &\approx \sum_{k=0}^{K-1} X_r(F_k, m) X_p^*(F_k) e^{j2\pi F_k t} \\ &= \alpha e^{-j2\pi F_0 \tau_m} \sum_{k=0}^{K-1} X_p(F_k) e^{-j2\pi F_k \tau_m} X_p^*(F_k) e^{j2\pi F_k t} \\ &= \alpha e^{-j2\pi F_0 \tau_m} \sum_{k=0}^{K-1} |X_p(F_k)|^2 e^{j2\pi F_k (t - \tau_m)} \end{aligned}$$

Considering a target in motion, note that this matched filter output peaks as $t = \tau_m$,

resulting in a scattering estimate of

$$\hat{\alpha} = \frac{1}{ME_p} \sum_{m=0}^{M-1} y_p(t = \tau_m, m) e^{j2\pi F_0 \tau_m} \tag{4.3}$$

where $\frac{1}{ME_p}$ is a scaling factor.

For a SAR system, the motion of a target in the scene will not be linear. To account for this, define $\mathcal{T}$ as an arbitrary set of propagation delays $\hat{\tau}_m$ that follows a particular motion profile. Applying this to the filter output results in a scattering estimate of

$$\hat{\alpha}(\mathcal{T}) = \frac{1}{ME_p} \sum_{m=0}^{M-1} y_p(t = \hat{\tau}_m, m) e^{j2\pi F_0 \hat{\tau}_m} \tag{4.4}$$

and bringing it back to frequency domain gives

$$\begin{aligned}
\hat{\alpha}(\mathcal{T}) &= \alpha \frac{1}{ME_p} \sum_{m=0}^{M-1} e^{j2\pi F_0 \hat{\tau}_m} e^{-j2\pi F_0 \tau_m} \sum_{k=0}^{K-1} |X_p(F_k)|^2 e^{j2\pi F_k (t-\tau_m)} \Big|_{t=\hat{\tau}_m} \\
&= \alpha \frac{1}{ME_p} \sum_{m=0}^{M-1} e^{j2\pi F_0 (\hat{\tau}_m - \tau_m)} \sum_{k=0}^{K-1} |X_p(F_k)|^2 e^{j2\pi F_k (\hat{\tau}_m - \tau_m)}
\end{aligned}$$

As the math shows, the result of the scattering estimate is a matched filter that applies both along pulses (M) and along frequency points (K), resulting in a unique peak for each motion profile. These matched filters are applied to the data via a *backprojection* method to find scattering estimates for each pixel in the desired scene, however detailed discussion of the implementation is out of the scope of this work.

4.2 Inertial Measurement Unit

When generating the motion profile in SAR processing, accurate positional information of the antenna throughout the flight path is required. To produce this data, an Inertial Measurement Unit (IMU) is used. The IMU uses a GPS antenna to geolocate itself via GPS satellites for coarse positional information. This data is then integrated with on-board fiber optic gyroscopes to fine tune positional information to achieve the final position measurement. This data is compared relative to the scene location and orientation to create the final motion profile.

The IMU used in this project is the NovAtel ISA-100C with a positional accuracy to approximately 1 cm. Data was also captured using a series of ADIS 16165 IMUs for an ongoing research effort. The IMU setup is shown in Figure 4.1.

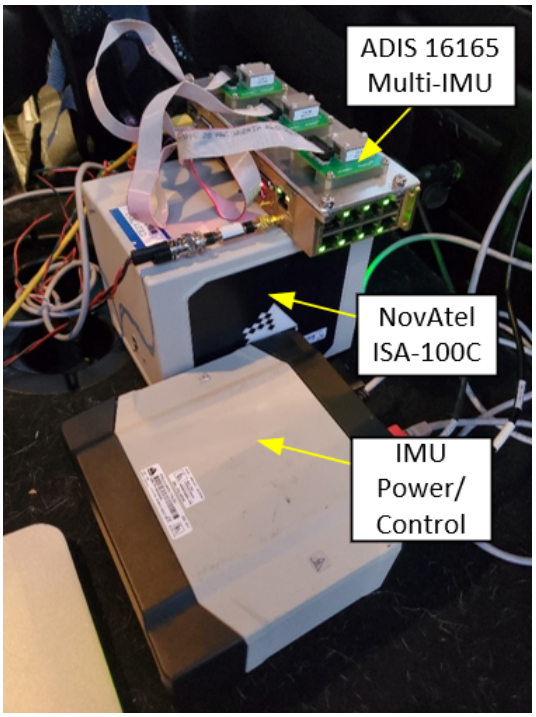

Figure 4.1: NovAtel IMU, its control/power unit, and the multi-IMU module.

4.3 Initial System Evaluation and Results

After fully integrating the system, the weight of the components came out as follows:

Table 4.1: System weight.

Part	Weight	Units
$Antennas$	1.5	lb
$PowerAmplifier$	2.5	lb
$Radar$	8	lb
IMU	17.4	lb
$Battery$	44.2	lb

Not included are the laptops which, in a fully integrated commercial system, would be replaced with a design specific interface. The total system weight of this hardware comes out to be approximately 74 lb.

From these weights, it can be seen that the primary contributors are the battery and the IMU equipment. The size of the X-Microwave system is approximately 10“ x 12”, which is far smaller than the connectorized system which took up nearly the entire 24“ x 36” cart space. As far as miniaturization goes, the project has been a success.

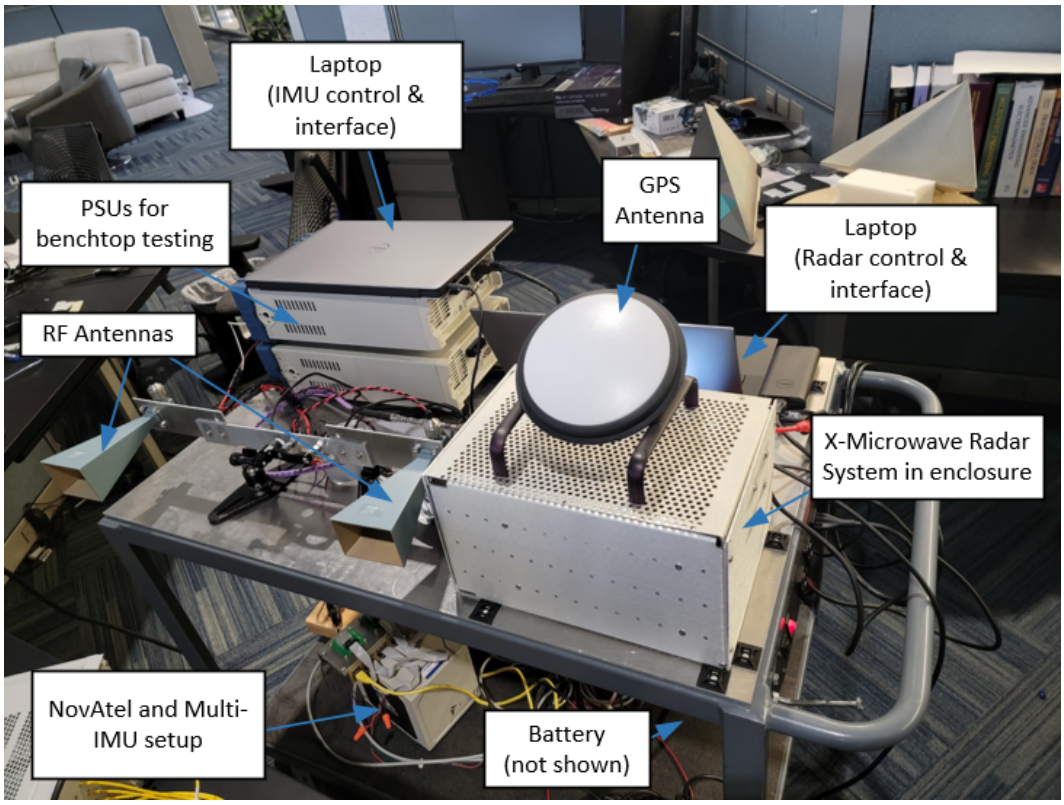

Figure 4.2: Cart setup for ground testing.

The ground test cart setup is shown in Figure 4.2. For the ground tests, the radar system was fixed to a cart, along with the RF antenna, IMU (and associated GPS antenna), and battery (used to supply all parts of the system). A Linux laptop was used to interface with the ARENA module and control the radar system itself, while a separate Windows laptop was used to set up and control the IMU system. For all of the ground testing, the system used a 3.012 kHz PRF with a 1 μs pulse width. The waveform was LFM with a bandwidth of 150 MHz, generated at a 2 GHz IF and upconverted to a 15 GHz RF. Approximately 45,000 pulses are typically collected on these ground tests, at 1.6 GSPS during the measurement window of 2 μs. The entire system, including IMU modules, is powered by a 12 V source and draws approximately 6.6 A during operation.

Loopback tests were conducted to verify system operation and sufficient system power level. Using approximately 80 dB of attenuation, the signal output to the receiver is clear to the eye before any signal processing, demonstrating that it is *close* to saturating the ADC, meaning near the maximum end of the input power level. The peak output power of approximately +34 dBm, after going through 80 dB of attenuation comes to -46 dBm into the receiver. Starting with this number, the and applying the simulated 57 dB of gain results in approximately +11 dBm, which is reasonably below the +16 dBm maximum input power calculated previously.

When taking measurements, unusual performance was observed when moving around components while this loopback test was running. The exact behavior was difficult to capture, but the problem was basically that the signal level was actively modulating when moving around components - an issue that would clearly cause problems if occurring during a system test. The power supply was examined first, since moving power supply lines seemed to cause the problems. After re-wiring the power supply lines and trying a loopback test yet again, the problem was still occurring. At this point it was noticed that the signal appeared to modulate differently with a "periodic" nature when moving an electrically reflective surface (such as a sheet of aluminum) near the system back and forth by a few centimeters. It was then apparent that the modulation was being caused by an isolation issue occurring when the system is simultaneously transmitting and receiving for the loopback testing. During the nominal loopback test, there was approximately 1 μs of delay through the system, which also happens to be the pulse width. Somewhere along the transmit path, the signal was coupling through air at the RF frequency to the receive side of the system, and physically moving an electrically reflective surface caused constructive/destructive interference in the signal with a wavelength of 2 cm, which tracks with the observed anomaly. An RF optical delay line was then used to isolate

the issue. When the system was delayed through the optical delay line by 10 μs, the problem vanished, since the signal was received long after the system was finished transmitting. After solving this coupling issue, the system appeared to function as expected and field testing could begin.

The system was first used to measure returns from corner reflectors to compare the new X-Microwave system to the old connectorized system. The use case for this test was effectively a side-looking SAR with a look-angle of 90 degrees from nadir. The scene was defined as a flat plane on the ground, level with the targets in question with the targets roughly in the center. Below is a comparison of the two systems set up in a similar configuration measuring corner reflectors, using an aperture of approximately 8 meters with approximately 45,000 pulses. First is an image produced by the connectorized system, followed by an image produced by the X-Microwave system using the ARENA backend.

The images demonstrate an increased target clarity at a further distance from the radar system. The SAR performance advantages of the X-Microwave system would include much-increased isolation performance due to the implemented shielding (despite the mutual coupling that was still observed in the current X-Microwave system). The image created using the old system is shown in Figure 4.3, and the image created using the X-Microwave system is shown in Figure 4.4.

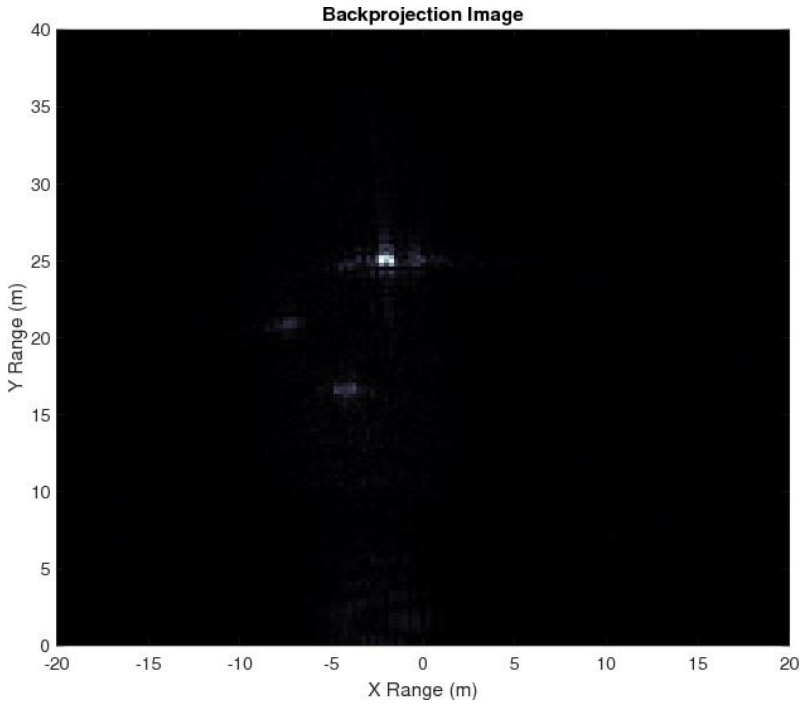

Figure 4.3: SAR image of three point (corner) reflectors using connectorized system.

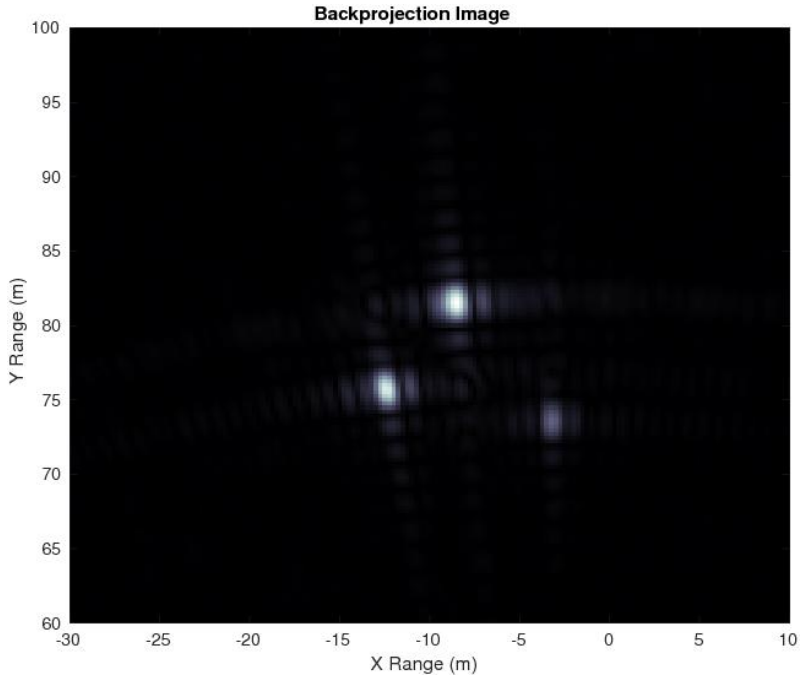

Figure 4.4: SAR image of three point (corner) reflectors using X-Microwave system.

The system was then tested by imaging a more complex scene with a similar setup configuration. The aperture for the next test was approximately 8 meters, across a road near the lab overlooking another building with vehicles in front of it used as targets. The use case for this test was again effectively a side-looking SAR with a look-angle of 90 degrees from nadir. The scene was defined as a flat plane on the ground, level with the vehicle targets with the structure at one edge of the scene. As the image demonstrates, the scatterers come in clear enough to discern individual targets and match up well with an overhead picture captured using the camera on a Ruko F11 drone. The SAR image is shown by itself in Figure 4.5, and with an accompanying overlay in Figure 4.6.

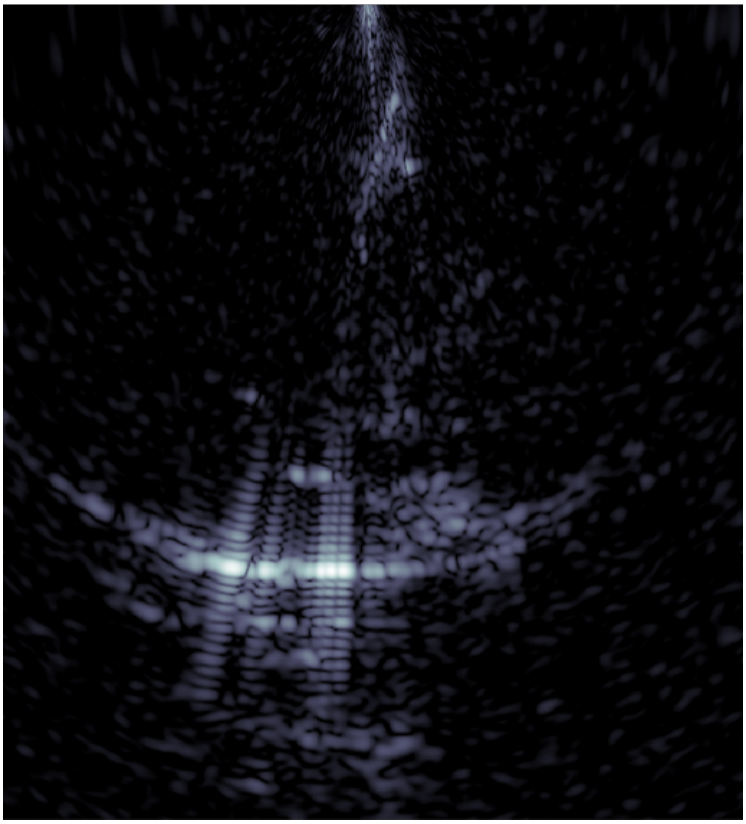

Figure 4.5: SAR image produced using the radar system designed in this work.

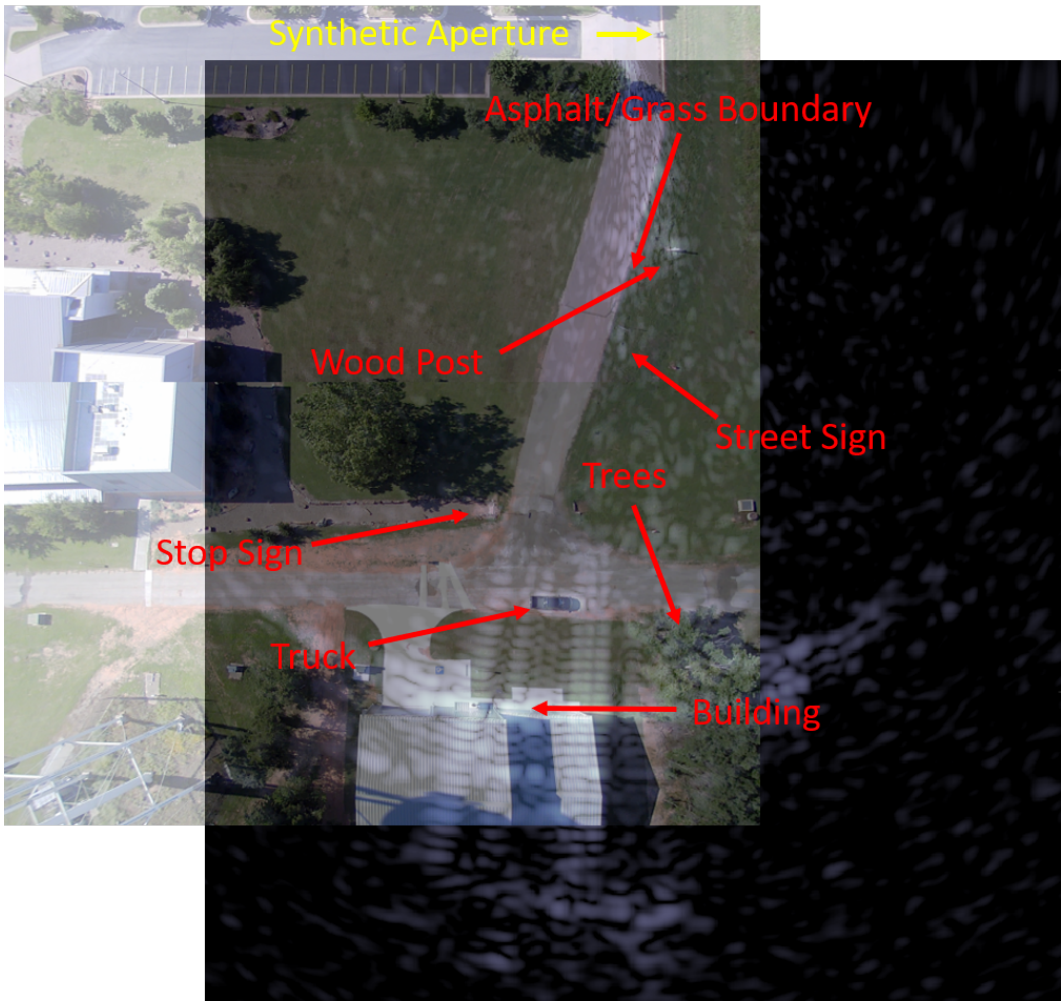

Figure 4.6: SAR image with overhead scene image overlay.

4.4 Flight Testing and Results

The radar flight tests were conducted with a Piper Warrior III, with the radar system itself held in the cargo bay, and the antennas fixed to the outside of the plane. This setup is shown in Figure 4.7.

Figure 4.7: System setup for flight test.

Now that the system had proven capable of producing images based on the ground test, flight tests were conducted to produce much larger and more compelling images from the air. The system was first used in a typical SAR configuration using a 30 degree from nadir look angle to produce an image of the ground at approximately a 300 m altitude along an flight track of approximately 1300 m. The result of this data collection is shown in Figure 4.8. The image appears to match the ground scene well and marking this as a good data capture.

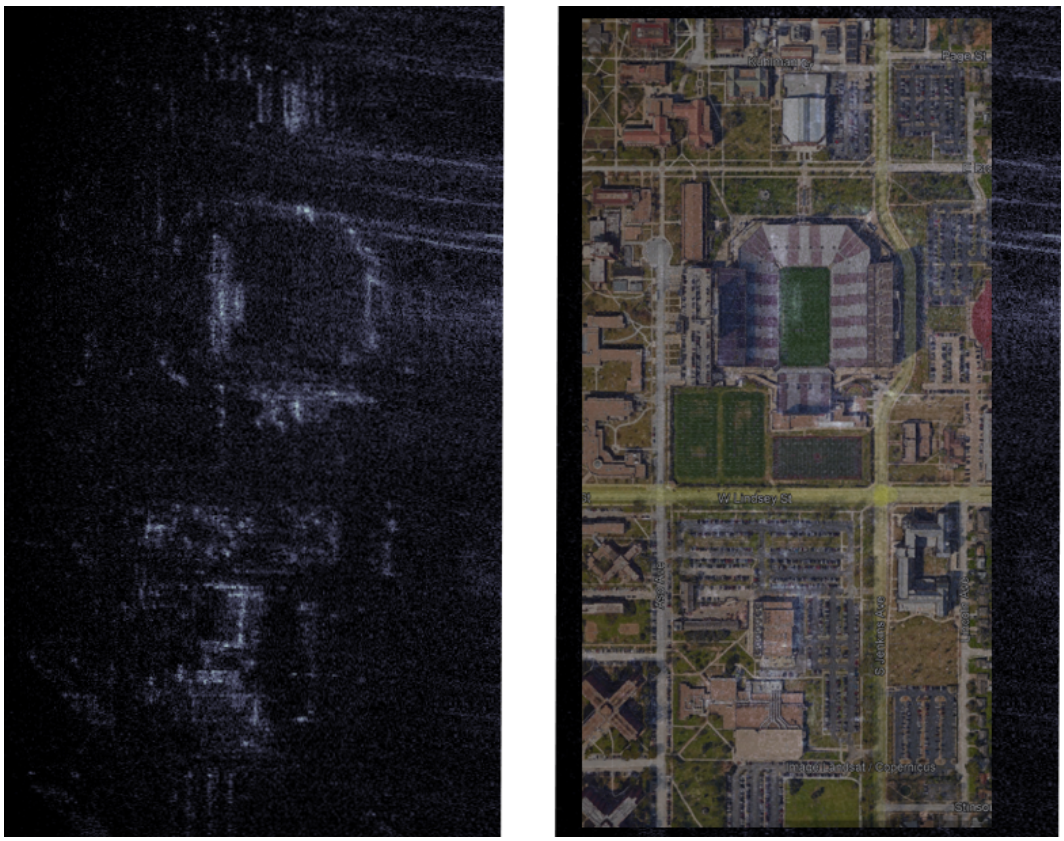

Figure 4.8: SAR image of Oklahoma Memorial Stadium with overlaid satellite image.

A flight was then planned to capture data which could be used in a VSAR application. On this second flight, the altitude was in the 600-750 meter range, with a flight path length of approximately 3200 meters. The antennas were positioned in a nadir-orientation (directly towards earth), and approximately 200,000 pulses worth of data were captured at 1.6 GSPS. The imaging plane used in the backprojection processing was re-mapped from flat on the ground, to orthogonal to the ground and parallel to the flight path, resulting in an image that is essentially an altitude profile.

To create a "ground truth" reference image for the VSAR configuration, the flight path was mapped out in Google Earth using GPS data from the IMU. The results of this are shown in Figure 4.9. The blue line overlaying the satellite image is the ground-projected trace of the flight path. The plot below the satellite image is the ground elevation profile which maps to the blue trace. This allows comparison of the SAR image directly to the elevation profile that it should follow.

As Figure 4.10 demonstrates, there appears to be a compelling match between the SAR collected data of the ground elevation and the elevation profile obtained from Google Earth. The altitude delta across the reference ground profile (starting at the second peak) is 22.5 m, which appears to match the image produced from the VSAR data capture. The altitude profile from the VSAR image appears to match closely with the elevation profile, verifying the accuracy of the measurements taken and proving the functionality of the system.

Figure 4.9: Visualization of the flight path using Google Earth, along with its associated ground elevation profile.

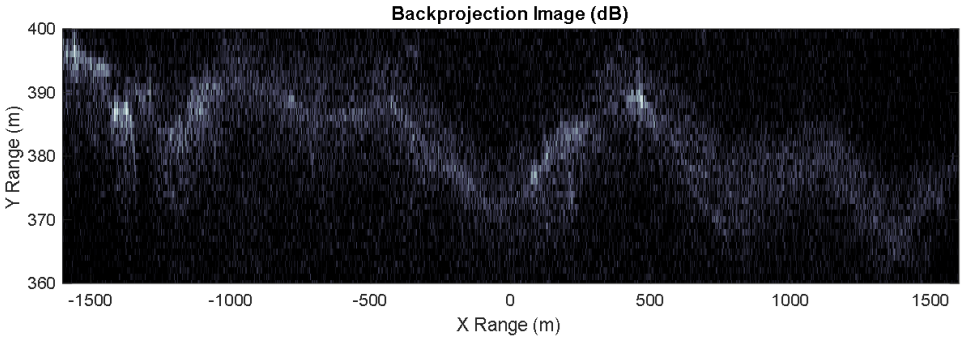

Figure 4.10: SAR used in VSAR configuration to produce image of the elevation profile of the flight path.

Chapter 5

Conclusions

5.1 Summary

In this work, the design process of a radar system prioritizing a low C-SWaP implementation was examined in detail. The high level system design based on the project requirements for the system was defined first. The project requirements were then used in conjunction with hardware which was previously allocated for the system to derive lower level requirements for the radar front-end. Moving on, each major component that was identified for the system which will drive system performance was inspected.

The hardware block diagram design of the front-end was designed and a cascade analysis was conducted to verify that the system is capable of meeting the derived requirements. Keysight's ADS was then used to conduct simulations to determine linear performance of the system using S-parameter models for each component and verify that the system is still capable of meeting requirements. Also in ADS, non-linear simulations were conducted to determine expected intermodulation products through the system and verify that filtering is sufficient to reject undesired products below the required SFDR level.

The system setup and test was then shown, first on the ground looking at point

reflectors, then on the ground creating an image. After verifying that the system is capable of clear imaging on the ground, data was captured from airborne tests and images were produced both from a standard side-looking SAR execution (with a 30 degree look-angle), then a nadir-looking VSAR application.

5.2 Conclusion

The objective of the work discussed in this thesis was to design a Ku-band radar system capable of SAR imaging with low C-SWaP in mind. Creating such a design which is simple to set up and tear down and is man-portable will provide great value for future research endeavors, as there is much room for expansion to accommodate project requirements. The radar system discussed in this work has been proven capable of capturing data sufficient to create clear SAR images, marking a decisive success for the system performance.

The cost of the front-end design was approximately $19,700, with the backend ARENA module coming out to approximately $24,000 for a total cost of the radar electronics of approximately $43,700. Use of X-Microwave components resulted in a reduced integration time and provided a circuit that was reconfigurable to optimize system performance based on system application.

The size of the X-Microwave radar (front-end and back-end) was approximately 12“ x 10” x 7“, far smaller than the previous connectorized design of 36” x 24“. The system was also sufficiently integrated to allow flight tests, with a total system envelope (excluding antennas and laptop) of approximately 16” x 24“ x 12”. Overall, the system was successfully integrated into a much smaller envelope, increasing execution capabilities substantially.

The weight of the radar came in at 8 lb, with the power amplifier coming in at

an additional 2.5 lb. The main drivers of the weight were the power supply (battery) at 44.2 lb and the IMU setup at 17.4 lb.

The overall current draw came in at approximately 6.6 A from a +12 V supply while the system was actively running. About half (3.5 A) was the radar, and half (3.1 A) was the IMU setup.

5.3 Future Work

There is room for improvement on a number of fronts for a following iteration of the design. The main probable path to take to reduce cost (per unit) would be increased unit count of a PCB design. As far as size, a preliminary PCB layout has been designed with an envelope of approximately 5.5” x 5.5” x 1”. Images of the design created in Altium are shown below.

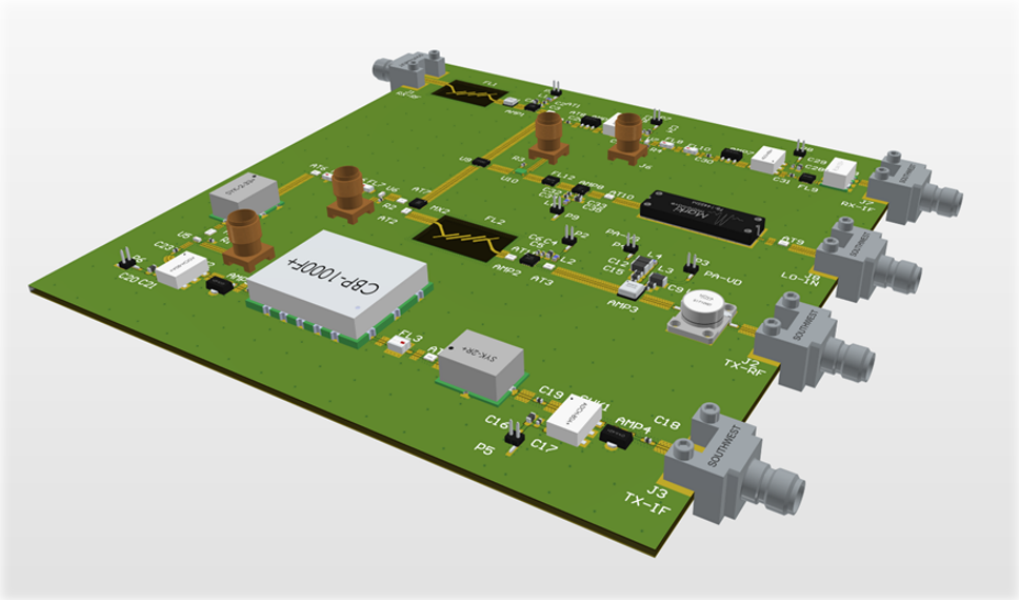

Figure 5.1: Isometric view of PCB design.

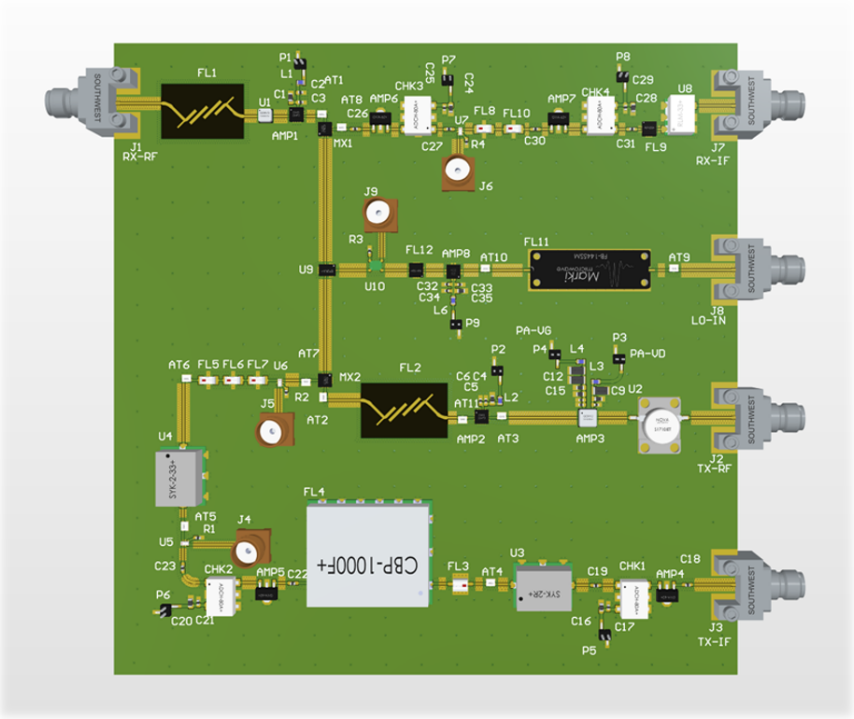

Figure 5.2: Top side of PCB design.

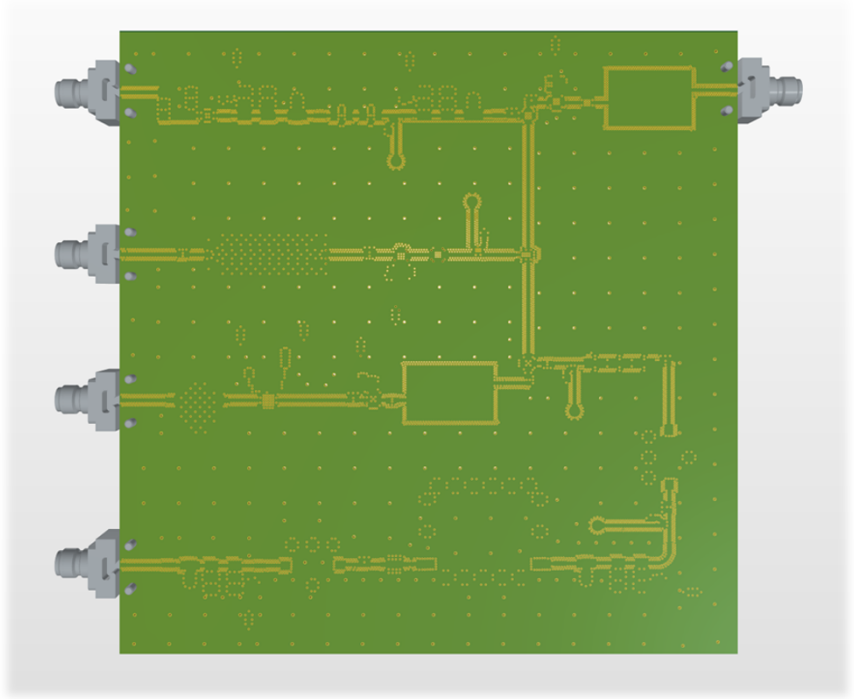

Figure 5.3: Bottom side of PCB design.

The Advanced Radar Research Center is conducting research to develop a very low C-SWaP IMU solution using smaller commercial IMU chips. As the research for the milti-IMU system is finalized, it may be utilized in future measurements using this radar system, substantially reducing the overall weight of the system.

The battery solution has not been optimized for weight. There appears to be a variety of options which could be utilized to power this system while substantially reducing weight, such as LiFePO4-type batteries with a high amount of stored energy for extended operation.

Currently the user interface and data storage is handled via two laptops to control the IMU and the radar itself. There is clear opportunity for C-SWaP reduction here, as one may utilize a much smaller, but more specialized, computing system to interface with the radar.

Finally, a new design could be implemented for the chassis containing the RF components. A smaller and more system-specific solution has been discussed, with one possibility being a 3D-printed design to maximize chassis size reduction with rapid prototyping capabilities.

References

[1] NASA 717 DC-8. NASA Jet Propulsion Lab. [Online]. Available: https://airsar.jpl.nasa.gov/dc8/dc8.html

[2] R. Kenney, "Design and Implementation of an All-COTS Digital Back-end for a Pulse-Doppler Synthetic Aperture Radar," Master's thesis, The University of Oklahoma, 2020.

[3] R. H. K. K. K. M. Y. H. H. S. J. W. McDaniel, "An all-COTS High Sampling Frequency Pulse-Doppler Imaging Radar," in *An All-COTS High Sampling Frequency Pulse-Doppler Imaging Radar*.

[4] M. I. Skolnik, *Introduction to Radar Systems*, 2nd ed. McGraw-Hill, 1980.

[5] M. A. Richards, *Fundamentals of Radar Signal Processing*, 2nd ed. McGraw-Hill Education, 2014.

[6] H. Zumbahlen. (2007) Basic Linear Design. Analog Devices. [Online]. Available: https://www.analog.com/media/en/training-seminars/design-handbooks/Basic-Linear-Design/Chapter4.pdf

[7] F. M. . C. Marki. (2010) Mixer Basics Primer: A Tutorial for RF and Microwave Mixers. Marki Microwave. [Online]. Available: https://www.markimicrowave.com/assets/appnotes/mixer_basics_primer.pdf

[8] A. W. Doerry, "Radar Receiver Oscillator Phase Noise," Sandia National Laboratories, Tech. Rep., 2018.

[9] A. W. Doerry, "Performance Limits for Synthetic Aperture Radar - second edition," Sandia National Laboratories, Tech. Rep., 2006.

[10] ZVE-3W-183+. Mini-Circuits. [Online]. Available: https://www.minicircuits.com/pdfs/ZVE-3W-183+.pdf/

[11] CMD192C5. Qorvo. [Online]. Available: https://www.custommmic.com/resources/cmd192c5-0418.pdf

[12] CMD192C5 X-Microwave Block. X-Microwave. [Online]. Available: https://www.xmicrowave.com/product/xm-a3e6-0804d/

[13] CMD264P3. Qorvo. [Online]. Available: https://www.custommmic.com/resources/cmd264p3-08-18-1.pdf

[14] CMD264P3 X-Microwave Block. X-Microwave. [Online]. Available: https://www.xmicrowave.com/product/xm-a9w8-0404d/

[15] AVA-183A. Mini-Circuits. [Online]. Available: https://www.minicircuits.com/pdfs/AVA-183A+.pdf

[16] AVA-183A X-Microwave Block. X-Microwave. [Online]. Available: https://www.xmicrowave.com/product/xm-b216-0404d/

[17] TGA2611-SM. Qorvo. [Online]. Available: https://www.qorvo.com/products/d/da004221

[18] TGA2611-SM X-Microwave Block. X-Microwave. [Online]. Available: https://www.xmicrowave.com/product/xm-b1m9-0404d/

[19] TGL2208-SM. Qorvo. [Online]. Available: https://www.qorvo.com/products/d/da004982

[20] TGL2208-SM X-Microwave Block. X-Microwave. [Online]. Available: https://www.xmicrowave.com/product/xm-a774-0404d/

[21] EP2KA. Mini-Circuits. [Online]. Available: https://www.minicircuits.com/pdfs/EP2KA+.pdf

[22] EP2KA X-Microwave Block. X-Microwave. [Online]. Available: https://www.xmicrowave.com/product/xm-b7p4-0404d/

[23] CMD178C3. Qorvo. [Online]. Available: https://www.custommmic.com/resources/cmd178c3_ver_1.5_1017.pdf

[24] CMD178C3 X-Microwave Block. X-Microwave. [Online]. Available: https://www.xmicrowave.com/product/xm-a5b6-0404d/

[25] ADF5355BCPZ. Analog Devices. [Online]. Available: http://www.analog.com/media/en/technical-documentation/data-sheets/ADF5355.pdf

[26] ADF5355BCPZ X-Microwave Block. X-Microwave. [Online]. Available: https://www.xmicrowave.com/product/xm-a741-0409d/

[27] XM-B9B4-1404D. X-Microwave. [Online]. Available: https://www.xmicrowave.com/product/xm-b9b4-1404d/

[28] L204XF4S. Knowles Capacitors. [Online]. Available: http://www.knowlescapacitors.com/getattachment/Products/Microwave-Products/Lowpass-Filters/L204XF4S-Datasheet.pdf.aspx?lang=en-US

[29] L204XF4S X-Microwave Block. X-Microwave. [Online]. Available: https://www.xmicrowave.com/product/xm-a2b8-0404d/

[30] HFCN-1600. Mini-Circuits. [Online]. Available: https://www.minicircuits.com/pdfs/HFCN-1600+.pdf

[31] HFCN-1600 X-Microwave Block. X-Microwave. [Online]. Available: https://www.xmicrowave.com/product/xm-a1d3-0204d/

[32] LFCN-2250 X-Microwave Block. X-Microwave. [Online]. Available: https://www.xmicrowave.com/product/xm-a1a5-0204d/

[33] XLF-252. Mini-Circuits. [Online]. Available: https://www.minicircuits.com/pdfs/XLF-252+.pdf

[34] XLF-252 X-Microwave Block. X-Microwave. [Online]. Available: https://www.xmicrowave.com/product/xm-a3f8-0404d/

[35] XLF-133. Mini-Circuits. [Online]. Available: https://www.minicircuits.com/pdfs/XLF-133+.pdf

[36] XLF-133 X-Microwave Block. X-Microwave. [Online]. Available: https://www.xmicrowave.com/product/xm-a3g9-0404d/

[37] FB-1300SM. Marki-Microwave. [Online]. Available: https://www.markimicrowave.com/Assets/datasheets/FB-1300SM.pdf

[38] FB-1300SM X-Microwave Block. X-Microwave. [Online]. Available: https://www.xmicrowave.com/product/xm-a7j1-1004d/

[39] J. W. McDaniel, "Ku-Band Synthetic Aperture Radar: System Parameters Study," The University of Oklahoma, Tech. Rep.